Disorganization of basement membrane zone architecture causes impaired melanocyte inhabitation in vitiligo

(15 words)

Fei Yang [1,2§], Lingli Yang [1§*], Yasutaka Kuroda [1,2], Sylvia Lai [1], Yoshito Takahashi [2], Tetsuya Sayo [2*], Takeshi Namiki [3], Kimiko Nakajima [4], Shigetoshi Sano [4], Shintaro Inoue [5], Daisuke Tsuruta [6] and Ichiro Katayama [1]

[1] Department of Pigmentation Research and Therapeutics, Graduate School of Medicine, Osaka Metropolitan University, Osaka 5450051, Japan

[2] Biological Science Research Laboratories, Kao Corporation, Odawara 2500002, Japan

[3] Department of Dermatology, Tokyo Medical and Dental University Graduate School and Faculty of Medicine, Tokyo 1138510, Japan

[4] Department of Dermatology, Kochi Medical School, Kochi University, Kochi 7838505, Japan

[5] Department of Cosmetic Health Science, Gifu Pharmaceutical University, Gifu 5011196, Japan

[6] Department of Dermatology, Graduate School of Medicine, Osaka Metropolitan University, Osaka 5458585, Japan

[§] These two authors contributed equally to this work: Fei Yang, Lingli Yang.

[*] Correspondence: yang.lingli@omu.ac.jp (L.Y.); sayou.tetsuya@kao.com (T.S.); Tel./Fax: +81-6-6556-7618 (L.Y.); Tel./Fax: +81-465-34-6111 (T.S.)

Keywords: fibroblasts; melanocyte; basement membrane; vitiligo; MMP2

Abbreviations: BM, basement membrane; BMZ, basement membrane zone; MMP2-Fb, MMP2-overexpressing fibroblasts; MMP2, matrix metalloproteinase 2.

Abstract (150 words)

Vitiligo is a common but puzzling skin disorder characterized by the selective loss of epidermal melanocytes due to unknown mechanisms. Here, we show patients with vitiligo have disruptions of basement membrane zone (BMZ) architecture including branched, fragmented, and multilayered lamina densa with increased numbers of dermal fibroblasts and overexpression of MMP2 in those cells. Extracts of vitiliginous skin showed increased MMP2 protein expression, with a large portion of the MMP2 proteins in the active form. Intradermal injection of MMP2-overexpressing fibroblasts in K14-SCF transgenic mice induced a vitiligo-like skin appearance and disappearance of melanocytes, which were reversed by coadministration of MMP2 inhibitors. These results suggest that disorganization of the BMZ driven by MMP2 overexpression in dermal fibroblasts may cause the impaired melanocyte inhabitation observed in vitiligo.

Introductions

Vitiligo is a puzzling disorder characterized by selective loss of epidermal melanocytes by an unknown mechanism[1]. Vitiligo was first described 3,500 years ago and is today a common skin disorder with an incidence of 1–2% wordwide[2, 3]. The most striking histological feature of vitiligo is the disappearance of melanocytes in the epidermis. The cellular and molecular mechanisms underlying melanocyte disappearance have attracted much interest from cell biologists and dermatologists. So far, many theories regarding the cause of melanocyte disappearance have been proposed, including autoimmune mechanisms, neural deficiencies, impaired redox status, and reduced melanocyte adhesion[4, 5]. A consensus on the true mechanism remains elusive.

In recent years, research on vitiligo pathogenesis has mainly focused on the importance of the IFNγ-CXCL9/10/CXCR3 axis. Autoreactive $CD8^+$ T cells and resident memory $CD8^+$ T cells are suggested to play an important role in the elimination of melanocytes in vitiliginous skin[4, 6]; however, compared with other chronic skin conditions, vitiligo often lacks clinical symptoms and overt signs of inflammation. Histologically, although limited lymphocytic infiltration is observed in the margin of early lesions, skin with established vitiligo lesions frequently displays unremarkable histopathological changes other than a near complete absence of melanocytes. These features make it difficult to understand why the characteristic white patches persist in the absence of overt infiltrates. There is no known cure for vitiligo, and the characteristic white patches have a substantial impact on patients'

quality of life. Clarification of the mechanism behind the loss of melanocytes in the absence of infiltration or severe inflammation may lead to new therapy options.

Epidermal melanocytes are specialized, pigment-producing cells derived from the neural crest. Under normal homeostatic conditions, they localize in the basal layer of the epidermis where they are maintained in a quiescent state and rarely proliferate, keeping a life-long stable ratio of 1:5 with basal keratinocytes[7]. Physiologically, dysregulation of homeostasis disturbs the epidermal-melanin unit and triggers pigmentary disorders[7, 8]. Melanocyte homeostasis is intricately regulated by epidermal keratinocytes, the surrounding stroma, and nearby dermal cells[9]. Cellular physiology and pathophysiology depend on both cell–cell interactions and cell–matrix interactions, and differentiated epidermal melanocytes are strictly localized at the basement membrane (BM) and cannot survive if they leave the basal layers, except in nevi or melanomas[10].

The BM is a thin sheet of highly specialized extracellular matrix[11, 12] located between the epidermis and the dermis that participates in diverse cellular functions including adhesion, proliferation, differentiation, and survival[13]. There are three layers within the BM: the lamina lucida, the lamina densa, and the anchoring fibrils. The lamina densa is a dense, colored layer approximately 30–60 nm in width that is closest to the underlying connective tissue. The anchoring fibrils are linked to the papillary dermis and localized in the lower part of the BM. Destruction of extracellular matrix macromolecules is seen in diseases such as arthritis[14], periodontal disease[15], and dermatological

disorders[16]; however, there has been little research on abnormal BM morphology in vitiligo[17, 18, 19, 20]. Because the BM provides structural support for keratinocytes and melanocytes, it is reasonable to hypothesize that structural abnormalities of the BM may have an impact on melanocyte disappearance in vitiligo.

Collagen IV is the most abundant BM component and serves as the backbone of the BM. Laminin, a matrix protein generated by keratinocytes and fibroblasts, is the second most abundant BM component[21]. In the BM, laminins are integrated into the type IV collagen scaffold by crosslinking to assemble the sheet-like BM complex[21]. Basal keratinocytes firmly adhere to the BM matrix via hemidesmosomes and focal adhesions[21]. Hemidesmosomes link intracellular keratin intermediate filaments to the underlying BM via integrin α6β4–laminin 332 binding and collagen XVII–collagen IV binding. Focal adhesions link intracellular actin filaments to the BM via integrin α3β1–laminin 511 binding[21].

Matrix metalloproteinases (MMPs) are a group of proteolytic enzymes that use zinc to control cell matrix composition. Metalloproteinases and the proteolytic breakdown of BM are essential for normal biological processes such as embryonic development, neuron growth, hair follicle cycling, bone remodeling, wound healing, and angiogenesis[22]. Dysregulated metalloproteinase expression leads to pathological conditions including inflammation, arthritis, cardiovascular diseases, nephritis, neurological diseases, pulmonary diseases, and cancer[22, 23]. MMP levels are elevated in various tissues

91 in autoimmune disorders[24], including brain tissue in autoimmune encephalomyelitis[25, 26], cerebrospinal
92 fluid in multiple sclerosis[27], synovial fluid in rheumatoid arthritis[28], and salivary glands in Sjogren's
93 Syndrome[29]. MMP2 was first reported by Liotta et al.[30], who found that an enzyme secreted by a
94 metastatic murine tumor cleaved type IV collagen, producing fragments. The enzyme did not attack
95 collagen types I, II, III, and V. When it was purified, the enzyme was found to consist of two forms of
96 approximately 72 kDa and 62 kDa, representing the pro and active forms, respectively[31].

97 We used electron microscopy, three-dimensional/organotypic culture, and mouse experiments to
98 reveal a novel mechanism to explain melanocyte disappearance from the BM in vitiligo. Compared
99 with healthy skin, lesional skin from patients with vitiligo displayed abnormalities in the structure and
100 components of the BM. The abnormalities were caused by fibroblasts that highly expressed MMP2,
101 which degraded BM matrix components and induced failure of melanocyte inhabitation. These
102 findings provide new knowledge about the etiology and pathogenesis of vitiligo and suggest a new
103 approach to vitiligo treatment.

Results

Basement membrane zone architecture is disorganized in vitiligo

To investigate the BM zone (BMZ) in vitiligo in detail, we performed an ultrastructural analysis using biopsy specimens from five healthy donors and five patients with generalized vitiligo (two stable, three progressive). We observed abnormal BM morphology in the samples of both stable and progressive vitiligo. As shown in **Fig 1a**, the BM of healthy skin contained intact lamina densa with high electron density, whereas the BM of vitiliginous skin contained branched and fragmented lamina densa, some of which were multilayered. Furthermore, the anchoring fibrils (**Fig 1a, red asterisks**) were distributed normally in the BM of healthy skin, but they were scattered and distributed in both the upper and the lower portion of the branched lamina densa in vitiliginous skin.

Next, we used immunofluorescence staining to investigate the expression and localization of BM proteins. Skin specimens from five healthy donors and 11 patients with generalized vitiligo (five stable, six progressive) were stained with antibodies against collagen IV (the main component of BM) and TRP1 (a melanocyte marker). In healthy skin, the BM had normal morphology (a thin continuous linear band of collagen IV) and a normal number and distribution of melanocytes (**Fig 1b**). By contrast, in vitiliginous skin, the BM had various abnormal morphologies, including obvious thickening (**Fig 1b, upper panel of Vitiligo-L**), severe disruption (**Fig 1b, middle panel of Vitiligo-L**), and multilayering (**Fig 1b, lower panel of Vitiligo-L**), accompanied by the disappearance of melanocytes.

We investigated the ultrastructural localization of collagen IV by immunoelectron microscopy using

123 an antibody against collagen IV. As expected, in an ultrathin section of healthy skin, we observed intact
124 BM, with collagen IV-labeled gold-particle deposits located close to the lamina densa (**Fig 1c, white**
125 **arrowhead in left panel**) in a continuous BM-like arrangement. By contrast, in an ultrathin section
126 of vitiliginous skin, we observed conspicuous structural alterations of the BM, with collagen IV-
127 labeled gold-particle deposits scattered across a wide area not only close to the normal lamina densa
128 area (**Fig 1c, white arrowhead in right panel**) but also near the branched structures (**Fig 1c, white**
129 **arrow**) and multilayered structures (**Fig 1c, white asterisk**) of lamina densa. These results revealed
130 that the BMZ architecture is disrupted in lesional vitiliginous skin.

131 **Matrix metalloproteinase 2 expression is elevated in the dermis of vitiliginous skin**

132 To ascertain why the BM structure was disrupted, we measured the expression levels of MMP2
133 (also known as gelatinase A) and MMP9 (also known as gelatinase B), the major proteolytic enzymes
134 capable of degrading BM collagen, in skin sections from patients with vitiligo. Immunofluorescence
135 staining was performed on frozen skin sections using anti-MMP2 antibody and anti-MMP9 antibody.
136 In comparison with healthy skin, lesional vitiliginous skin showed modestly increased MMP9
137 expression and dramatically increased MMP2 expression in the upper dermis (**Fig 2a and 2b**).
138 Fibroblasts[32] and vascular endothelial cells[33] are the main MMP2-producing cells in human skin. To
139 determine which cell types were responsible for the high MMP2 production in vitiliginous skin, we
140 performed immunolocalization studies on vitiliginous and healthy skin tissues. Frozen sections from

141 five healthy controls and 11 patients with vitiligo were incubated with anti-MMP2 antibody and then
142 counterstained with anti-HSP47 (a skin fibroblast marker) and anti-CD31 (a marker of endothelial
143 cells) antibodies. Remarkably, the number of fibroblasts was significantly increased in the vitiliginous
144 skin; however, there was no appreciable difference in the number of endothelial cells between the
145 vitiliginous skin and the healthy skin (**Fig 2c and 2d**). In addition, the percentage of MMP2-positive
146 fibroblasts was almost four times higher in the vitiliginous skin than in the healthy skin, but there was
147 no significant difference in the percentage of MMP2-positive endothelial cells (**Fig 2e and 2f**). To
148 determine whether MMP2-positive fibroblasts were present in the area surrounding the BM, we
149 performed immunofluorescent labeling with anti-MMP2 antibody and counterstaining with anti-
150 HSP47 and anti-collagen IV (a marker of BM) antibodies. This revealed that in the vitiliginous skin,
151 but not the healthy skin, MMP2-positive fibroblasts were located near the BM (**white arrowheads in**
152 **Fig 2g**) and also went through the BM to reach the epidermis (**white arrows in Fig 2g**).
153 Next, we examined the activity of MMP2 by western blot using skin lysates from three patients
154 with vitiligo (one stable, two progressive) and three healthy controls. In the healthy skin, MMP2 was
155 slightly expressed and mainly in the pro (inactive) form; however, in the vitiliginous skin, MMP2 was
156 highly expressed and mainly in the active form (**Fig 2h and 2i**). These results revealed that vitiliginous
157 skin had increased MMP2 in the dermis, produced mainly by upper-dermis fibroblasts, and the MMP2
158 was mainly in the active form, suggesting that MMP2-induced BM degradation might be involved in

159 the production of vitiligo lesions.

160 **Overexpression of MMP2 in dermal fibroblasts results in melanocyte disappearance**

161 **in reconstructed human skin equivalents and human *ex vivo* cultured skin explants**

162 To determine whether damage to the BM precedes the disappearance of melanocytes in vitiliginous

163 skin, we developed an *in vitro* three-dimensional (3D) skin equivalent model. In each 3D skin

164 equivalent, half of the collagen gel in the dermis layer was prepared with mock-transfected fibroblasts

165 (Mock-Fbs) and half with MMP2-overexpressing fibroblasts (MMP2-Fbs) (**Fig 3a**). Once the

166 structured collagen gel was established, melanocytes and keratinocytes were uniformly seeded on top

167 of the gel. After 1 week of air-lift culture, macroscopically pigmented skin developed on the part of

168 the gel prepared with Mock-Fbs, whereas no pigmentation developed on the part of the gel prepared

169 with MMP2-Fbs (**Fig 3b**). Immunofluorescent staining of melanocytes and BM revealed that in the

170 3D skin equivalents prepared with Mock-Fbs, the BM had a typical thin line morphology, and

171 melanocytes were uniformly distributed among the keratinocytes in the basal layer; however, in the

172 3D skin equivalents prepared with MMP2-Fbs, the BM appeared damaged, and the melanocytes had

173 disappeared (**Fig 3c**).

174 Next, we created an *ex vivo* subcutaneous injection model in which Mock-Fbs or MMP2-Fbs were

175 subcutaneously inoculated into cultured, full-thickness, fresh skin explants. To track the injected

176 fibroblasts, we labeled them with PKH fluorescence cell-membrane labeling dye (**Fig 3d**). After *ex*

177 *vivo* skin culture, the skin explants were stained with anti-Melan-A and anti-collagen IV antibodies.
178 In contrast to skin explants injected with PBS or Mock-Fbs, skin explants injected with MMP2-Fbs
179 displayed obvious BM disruption and melanocyte disappearance (**Fig 3e**). These results suggest that
180 increased MMP2 expression by dermal fibroblasts is a key factor in melanocyte disappearance in
181 vitiligo.

182 **Melanocyte disappearance results from decreased adhesion to the BM**

183 We performed immunofluorescent staining to further examine the disappearance of melanocytes
184 from the damaged BM. The melanocytes were anchored to the BM and located on the basal layer in
185 the 3D skin equivalents prepared with Mock-Fbs, (**Fig 4a, Mock-Fb**); however, they were detached
186 from the BM and tended to be located at the suprabasal layer in the marginal zone of the depigmented
187 3D skin equivalents (**Fig 4a, MMP2-Fb (MZ)**). These detached melanocytes were negative for
188 cleaved-caspase 3 (**Fig 4a**), suggesting that apoptotic events were not involved in their disappearance.
189 These data suggested that abnormal adhesion between melanocytes and the BM was involved in the
190 melanocyte disappearance, so we next focused on melanocyte adhesion.

191 Cells in the basal layer of the epidermis are bound to the BM mainly through integrins, but the
192 mechanistic details of melanocyte adhesion to the BM are still unknown. Melanocytes have been
193 reported to express integrin β1 both *in vitro* and *in vivo*[34]. In addition, discoidin domain receptor 1
194 (DDR1), a membrane protein, was recently reported to bind collagen IV and mediate the adhesion of

195 melanocytes to BM[35]. Furthermore, some studies reported that loss of melanocytes in vitiligo resulted
196 from decreased DDR1 expression in melanocytes[36, 37]. We examined adhesion patterns between
197 melanocytes and the BM matrix using *in situ* proximity ligation assay (PLA), an antibody-based
198 technology that enables the visualization of protein–protein interactions. Specifically, we examined
199 integrin β1–laminin-binding and DDR1–collagen IV binding in 3D skin equivalents. In the PLA, when
200 a pair of specific primary antibodies (DDR1 and collagen IV; integrin β1 and laminin) is in close
201 proximity, complementary DNA strands on a corresponding pair of secondary antibodies with PLA
202 probes engage in rolling circle amplification and generate a single fluorescent signal *in situ*, indicating
203 the presence of the corresponding protein–protein interaction (**Fig 4b**). We detected PLA signals for
204 DDR1–collagen IV and integrin β1–laminin along the basal layer of epidermis in 3D skin equivalents
205 prepared with Mock-Fbs (**Fig 4c**); however, in the marginal zone of depigmented 3D skin equivalents
206 prepared with MMP2-Fbs, the DDR1–collagen IV and integrin β1–laminin PLA signals were
207 markedly decreased (**Fig 4c and 4d**).

208 We confirmed the detachment of melanocytes from the BM by *in situ* PLA of perilesional skin from
209 patients with vitiligo (**Fig 5a**). Immunofluorescence staining did not show any difference in the
210 expression levels of DDR1, collagen IV, integrin β1, and laminin between healthy skin and perilesional
211 vitiliginous skin (**Fig 5b, 5c, and 5f**). We visualized the adhesions between melanocytes and the BM
212 matrix by *in situ* PLA and co-immunohistochemistry staining of melanocytes with anti-TRP1 antibody

213 (**Fig 5d and 5e, white rectangle box in right lower panel**). In melanocytes of healthy skin, integrin
214 β1–laminin interactions were much more predominant than DDR1–collagen IV interactions; however,
215 both interactions were significantly reduced in melanocytes of perilesional vitiliginous skin (**Fig 5e**
216 **and 5g**). These data demonstrated that the two major melanocyte–BM adhesion patterns were
217 strikingly weakened in vitiliginous skin (**Fig 5h**).

218 In contrast to the detachment of melanocytes, we did not observe detachment of keratinocytes
219 (blistering) in perilesional vitiliginous skin despite a weakened focal adhesion signal (integrin β1–
220 laminin binding) around basal keratinocytes (**Fig 4c; Fig 5e**). Therefore, we examined the expression
221 levels and binding signals of hemidesmosome proteins. There was no difference in the expression
222 levels of integrin α6 and laminin between healthy skin and lesional vitiliginous skin (**Fig 6a and 6c**);
223 however, the expression levels of collagen XVII and collagen IV were significantly increased in the
224 lesional vitiliginous skin (**Fig 6b and 6c**). We used *in situ* PLA to examine the hemidesmosome
225 adhesion signal between basal keratinocytes and BM matrix (**Fig 6d**). In basal keratinocytes of healthy
226 skin, integrin α6–laminin interactions were much more predominant than collagen XVII–collagen IV
227 interactions (**Fig 6e and 6f**). By contrast, in basal keratinocytes of vitiliginous skin, the integrin α6–
228 laminin interaction was dramatically reduced, whereas the collagen XVII–collagen IV interaction was
229 strikingly increased (**Fig 6e and 6f**). These results indicated that the adhesion patterns between basal
230 keratinocytes and the BM were strikingly altered in lesional vitiliginous skin (**Fig 6g**), and a

231 compensatory increase in hemidesmosome adhesion via collagen XVII–collagen IV binding may be
232 the reason there was no skin blistering.

233 **Decreased melanocyte adhesion to the BM is caused by abnormal BM architecture**

234 The expression levels of DDR1, collagen IV, integrin β1, and laminin were similar between
235 vitiliginous and healthy skin, but the vitiliginous skin displayed decreased DDR1–collagen IV and
236 integrin β1–laminin interactions (**Fig 5**). To clarify what caused the reduction of these interactions, we
237 assessed the physical distance between the melanocytes and the BM using electron microscopy (**Fig**
238 **7a**). As basal cells are known to attach to the lamina densa of the BM, we measured the width of the
239 lamina lucida (the distance between the basal cell plasma membrane and the lamina densa) in healthy
240 skin and vitiliginous skin, but we unexpectedly found no difference between healthy skin and lesional
241 vitiliginous skin (**Fig 7a and 7c**). We then performed immunoelectron microscopy to determine
242 whether the decreased binding was due to aberrant localization of adhesion molecules. In healthy skin,
243 laminin, the predominant adhesion molecule on the BM responsible for melanocyte binding, was
244 clearly distributed along and confined to the lamina densa; however, in lesional and perilesional
245 vitiliginous skin, laminin was diffusely spread in the lamina densa and the beneath the disorganized
246 BM architecture (**Fig 7b**). Furthermore, the amount of laminin confined in the lamina densa was
247 markedly reduced in vitiliginous skin compared with that in healthy skin (**Fig 7b and 7d**). These data
248 suggest that laminin was aberrantly distributed in the vitiliginous skin, and the disorganized BMZ

249 architecture made it difficult for laminin to bind with integrin β1 on epidermal melanocytes.

250 **Inhibition of MMP2 reversed depigmentation in a novel mouse model of vitiligo**

251 **based on subcutaneous inoculation of MMP2-Fbs.**

252 We used K14-SCF transgenic mice characterized by the retention of melanocytes in the epidermis

253 to examine skin color changes in vitiligo. Murine Mock-Fbs and MMP2-Fbs were subcutaneously

254 transplanted into the back skin of K14-SCF mice (**Fig 8a**). One week after transplantation, no color

255 change was observed on the backs of mice transplanted with Mock-Fbs; however, depigmentation

256 spots were observed on the backs of mice transplanted with MMP2-Fbs (**Fig 8b**). Skin tissue from the

257 mice was subjected to immunofluorescence staining. Mice transplanted with Mock-Fbs or MMP2-Fbs

258 had many more fibroblasts in their skin tissues than control mice injected with PBS (**Fig 8c**).

259 Furthermore, skin tissues from mice with Mock-Fb transplantation contained epidermal melanocytes

260 and intact BM, whereas those from mice with MMP2-Fb transplantation contained no epidermal

261 melanocytes and had disrupted BM structure (**Fig 8c**). These data indicated that the subcutaneous

262 MMP2-Fb transplantation in K14-SCF mice provided a vitiligo-like depigmentation model. Next, to

263 determine whether inhibition of MMP2 could reverse the vitiligo-like depigmentation, we

264 subcutaneously co-injected MMP2-Fbs and an MMP2 inhibitor, either SB-3CT or tanomastat, into the

265 back skin of K14-SCF mice (**Fig 8d**). Compared with PBS as a control, both SB-3CT and tanomastat

266 remarkably inhibited the depigmentation of back skin (**Fig 8e and 8f**). These data suggest that

267 melanocytes disappeared from the basal layer of the depigmented epidermis as a consequence of

268 MMP2-induced disruption of the BM structure.

Discussion

The BM of vitiliginous skin has been shown to be morphologically thickened[17, 18], damaged[19], or branched[20], but it is unknown how the BM structure is disrupted and what role BM disruption plays in the pathophysiology of vitiligo. We confirmed the abnormal BM structure in vitiliginous skin and, furthermore, that the disorganized BMZ prevents melanocytes from adhering to the BM via integrin β1–laminin binding. Moreover, we discovered that the disorganized BM architecture is caused by increased MMP2 expression in dermal fibroblasts. MMP2-Fbs implanted in 3D skin equivalents and *ex vivo* cultured skin explants showed BM structural disruption and melanocyte detachment. K14-SCF mice developed vitiligo-like skin lesions after subcutaneous inoculation with MMP2-Fbs, and treatment with MMP2 inhibitors successfully reduced the depigmentation in these mice.

Melanocyte floating and defective melanocyte adhesion in vitiligo were described previously[38, 39], but the majority of previous studies focused on melanocyte–keratinocyte adhesion. Few investigations have looked at melanocyte–BM adhesion. We verified melanocyte detachment in vitiligo but found that neither the expression levels of melanocyte adhesion molecules nor the expression levels of BM proteins were decreased. Instead, immunoelectron microscopy, histo-immunofluorescence staining, and PLA analyses revealed that the reduction in melanocyte adhesion was due to disorganization of the BMZ architecture. These findings imply that the detachment of melanocytes in vitiligo is caused by an aberrant spatial distribution of adhesion molecules in the BM. In contrast to the decreased

287 adhesion and detachment of melanocytes, we did not observe any detachment of keratinocytes (i.e.,
288 blistering), which suggests that a powerful compensating mechanism in keratinocytes enables them to
289 adhere to the BM via collagen XVII and other molecules in hemidesmosomes, even when the
290 distribution of laminin is aberrant. Our ultrastructural investigations of vitiliginous skin confirmed the
291 existence of hemidesmosomes in basal keratinocytes. It is well known that there are no
292 hemidesmosome complexes in melanocytes, as these structures are exclusive to keratinocytes[40]. The
293 attachment of melanocytes to the BM is considerably weaker than that of keratinocytes and is mediated
294 by integrin β1–laminin binding[34] and DDR1–collagen IV binding[35]. Differentiated human
295 melanocytes are restricted to the BM, and their continued attachment to the BM is essential for their
296 survival, as they cannot survive in the upper epidermal layers unless they are changed into nevi or
297 melanomas[35]. Several studies hypothesized that melanocytes disappear in vitiligo because of weak
298 attachment to the epidermal BM, and they found that expression of the melanocyte–BM adhesion
299 molecule DDR1 was decreased in vitiligo[36, 37]. However, our *in situ* PLA study demonstrated that the
300 predominant adhesion between melanocytes and the BM is due to integrin β1–laminin binding, which
301 was dramatically reduced in vitiliginous skin. The protein expression levels of DDR1, integrin β1,
302 laminin, and collagen IV were unchanged in vitiliginous skin, which may explain why the reduced
303 integrin β1–laminin binding was not uncovered previously. Our findings suggest that structural
304 abnormality of the BM, rather than altered expression levels of adhesion molecules, was mostly

305 responsible for the decreased adhesion of melanocytes.

306 The two main MMPs that break down epidermal BM components are MMP2 and MMP9[23, 41].
307 MMP2 was dramatically elevated in the dermis of lesional vitiliginous skin, regardless of whether the
308 vitiligo was stable or progressive. Additionally, MMP9 expression was slightly increased in the dermis
309 of vitiliginous skin. Recent research revealed decreased E-cadherin expression in melanocytes[39] and
310 increased MMP9 expression in the epidermis of lesional vitiliginous skin[42], suggesting that reduced
311 E-cadherin levels in melanocytes and MMP9-induced breakdown of E-cadherin on keratinocytes and
312 melanocytes may cause melanocyte detachment in vitiligo. Our results show, however, that for
313 melanocytes to inhabit the skin's basal layer, they must adhere not only to neighboring keratinocytes
314 but also to the BM. In addition, MMP9 should affect not only cell–cell adhesion but also BM assembly.
315 Reports investigating *in vitro* cultured human melanocytes[43] and immortalized mouse melanoblasts[44]
316 demonstrated that reduced MMP2 expression in those cells was associated with cell migration and
317 might therefore be involved in the pathogenesis of vitiligo. However, in light of the aberrant BM
318 structure that we observed in vitiliginous skin, increased expression of MMP2 in dermal fibroblasts is
319 probably the most important event in vitiligo pathogenesis *in vivo*.

320 MMP2 is expressed constitutively by many cell types in culture. In adult tissues, MMP2 has been
321 identified in keratinocytes, skin fibroblasts, chondrocytes, osteoblasts, endothelial cells, monocytes,
322 and a number of other cell types[22]. Our immunolocalization analyses demonstrated that the majority

323 of the increase in MMP2-positive cells in vitiliginous skin was due to MMP2-expressing dermal
324 fibroblasts. In agreement with this, a recent study using single-cell analysis of lesional vitiliginous
325 skin revealed that dermal fibroblasts were associated with the loss of melanocytes[45]. Several
326 researchers have noted abnormal dermal fibroblasts in lesional vitiliginous skin[45, 46]. Kovacs et al.
327 observed that dermal fibroblasts in vitiliginous skin had a myofibroblast phenotype and a propensity
328 for premature senescence[47]. There is growing evidence that dermal fibroblasts contribute to the defects
329 associated with melanocytes in vitiligo, although their exact role remains unclear. It is currently
330 generally accepted that vitiligo is an autoimmune disease resulting from the destruction of melanocytes
331 by melanocyte-specific autoreactive $CD8^+$ T lymphocytes, and animal models of vitiligo have been
332 established accordingly[4, 45]. Despite that, patients with vitiligo frequently lack obvious inflammatory
333 clinical signs, so we looked for a mechanism other than direct immune cell participation. Our findings
334 enabled us to establish a new alternative mouse model of vitiligo based on subcutaneous injection of
335 MMP2-Fbs, which may provide new insights into pathomechanisms of non-immune cell-mediated
336 vitiligo.

337 MMP2 expression was elevated in dermal fibroblasts of vitiliginous skin, but the underlying reason
338 is unknown. There are many reports on paracrine modulation of MMP2 expression. Numerous
339 cytokines that are increased in lesional vitiliginous skin, including interleukin (IL)-1β[48, 49], IL-6[48],
340 tumor necrosis factor (TNF)-α[49, 50], and TGF-β[51, 52], have been reported to stimulate MMP2 expression.

341 Destruction of extracellular matrix macromolecules is seen in other diseases such as arthritis[14],
342 periodontal disease[15], and dermatological disorders[16], and invading inflammatory cells exacerbate the
343 pathogenesis of those diseases. These invading immune cells are thought to play an etiologic role
344 through their ability to produce cytokines that induce MMP expression in resident mesenchymal cells[53].
345 Damage to the epidermal BM alters interactions between epidermal keratinocytes and the
346 extracellular matrix[54]. Epidermal keratinocytes interact with extracellular matrix components such as
347 proteolytic fragments or cleavage sites (neoepitopes) in the surrounding stroma, which affects
348 epidermal homeostasis and keratinocyte phenotypes[12, 54, 55]. There is emerging evidence that
349 keratinocytes in lesional vitiliginous skin are genetically and biologically distinct from normal cells[46,
350 56, 57, 58]. We observed epidermal thickening in lesional vitiliginous skin in accordance with previous
351 histological findings[56, 59], but the mechanisms responsible for the fundamental abnormalities in
352 keratinocytes during vitiligo development remain unknown. Previous studies indicated that under
353 pathological conditions, extensive BM destruction results in enhanced release of cytokines in the
354 epidermis[54, 55, 60]. We found that disruption of the BMZ architecture altered the expression pattern of
355 adhesive molecules in basal keratinocytes, and the cytokines IL-1β, TGF-β1, TNF-α, and IL-6 were
356 highly expressed in the epidermis of vitiliginous skin lesions (**Extended Data Fig 1**). This cytokine
357 expression from epidermal keratinocytes might upregulate MMP2 expression in dermal fibroblasts
358 through paracrine regulation.

359 We also detected elevated MMP2 expression in dermal fibroblasts in stable vitiligo. We believe that
360 there may be a vicious cycle in which MMP2 destroys BM, and the consequent disruption of the BM
361 alters the phenotype of keratinocytes, resulting in cytokine production, which in turn upregulates
362 MMP2 expression in fibroblasts. When the normal BM healing process is interrupted, a pathological
363 vicious cycle of cytokine and protease release occurs, leading to the development of a permanent and
364 intractable pathological skin phenotype, such as stable vitiligo. The use of skin needling and laser
365 ablation in combination with phototherapies or topical medicines such as steroids, tacrolimus, and 5-
366 fluorouracil to treat stable vitiligo has shown satisfying results[61, 62, 63]. Stimulation of the dermis by
367 needling or laser ablation may induce biological changes in dermal fibroblasts, BM, and keratinocytes
368 that halt the pathogenic vicious cycle and repair the BMZ. The vicious cycle described here may
369 explain why melanocytes cannot return to the BM for a long time after they disappear, but it remains
370 unclear what triggers the initial event in the cycle. As the body's first line of defense, the NLRP3 and
371 NLRP1 inflammasomes are activated in response to various external stimuli, such as oxidative stress,
372 UV radiation, chemical agents, extracellular ATP, and microbial dysbiosis, and the cytokines IL-1β,
373 IL-6, and TNF-α consequently become elevated in the epidermis[64, 65]. The infiltrating lymphocytes
374 and other inflammatory cells that have been detected in the early initial stage of vitiligo may also be
375 capable of producing these cytokines. Ultimately, the cytokines may induce MMP2 expression in
376 dermal fibroblasts and initiate the vicious cycle of vitiligo development. Nonetheless, further research

377 is required to test this hypothesis.

378 We found that MMP2 expression was increased in protein extracts of full skin from vitiligo lesions
379 compared with that in protein extracts of healthy skin. The MMP2 in the skin extracts was mainly the
380 active 62-kDa form, indicating that the latent (pro) form of MMP2 in the dermis of lesional skin is
381 activated locally. Pro-MMP2 is known to be activated by TIMP-2, MT1-MMP, organomercurials, and
382 several proteases, including MMP7 and MMP3[22]. Further investigation is needed to determine whether
383 or not these are involved in the MMP2 activation in lesional vitiliginous skin.

384 Therapeutically, restoring the BM is the most important issue for melanocyte reinhabitation.
385 Pharmacologic interventions (e.g., anti-inflammatory medications or selective inhibitors of signaling
386 pathways) or molecular biological interventions (e.g., natural MMP2 inhibitors, monoclonal
387 antibodies, or siRNAs) that seek to modulate the expression or activation of MMP2 may have an
388 impact on the prevention and treatment of vitiligo. For example, steroids and selective inhibitors of
389 the IL-1β, TGF-β, TNF-α, and IL-6 signaling pathways may be partially effective for vitiligo treatment.
390 JAK inhibitors not only inhibit the production of cytokines by infiltrating $CD8^+$ T lymphocytes but
391 also have the ability to block some of the cytokine pathways in fibroblasts, which may make them
392 effective in vitiligo treatment. However, to successfully cure vitiligo, MMP2 expression should be
393 restored to a normal level. The use of MMP2 inhibitors, which are currently being evaluated in clinical
394 trials, is a promising therapeutic option for vitiligo; however, the systemic administration of MMP2

395 inhibitors may serve as a double-edged sword that promotes tissue healing and disturbs melanocyte
396 homeostasis. Therefore, it is crucial to suppress MMP2 with a selective inhibitor at an appropriate
397 dosage and preferably via local administration (e.g., topical application) to reduce potential side effects.
398 In summary, fibroblasts in the dermis of lesional vitiliginous skin express high levels of MMP2,
399 which disrupts the BM architecture, leading to a breakdown of the integrin β–laminin interactions that
400 provide the main adhesion between melanocytes and the BM. As a result, melanocytes detach from
401 the BM and disappear from the epidermis. The impairment of BM structure may lead to functional
402 changes in epidermal cells and induce keratinocyte abnormality, promoting melanocyte disappearance
403 by stimulating dermal fibroblasts, as summarized in **Fig 9**. These findings shed new light on the
404 pathogenesis of vitiligo. It appears that a disorganized BM caused by MMP2 from dermal fibroblasts
405 is responsible for the loss of melanocytes in vitiligo. Our *in vivo* results suggest that MMP2
406 suppression may have therapeutic implications for vitiligo; however, the MMP2-Fb–induced
407 depigmentation in 3D skin equivalents, *ex vivo* skin explants, and a mouse model was inadequate to
408 examine chronic changes in epidermal keratinocytes. Another limitation of this study is that only
409 MMP2 and MMP9 were examined. Other proteinases and endoglycosidases from dermal cells, such
410 as macrophages and mast cells, have the potential to degrade the BMZ, and it is possible that cytokines
411 and chemokines from abnormal keratinocytes alter these cells, thereby indirectly affecting the
412 phenotype of fibroblasts. Further research is needed to discover whether additional factors and cells

413 contribute to the BMZ disruption in vitiligo.

Figure Legends

Figure 1. Disorganization of basement membrane zone architecture in vitiligo

a, Representative ultrastructural images of ultrathin sections of skin from five healthy controls and five patients with generalized vitiligo. In the right panel, the areas of epidermis and dermis are represented by Epi and Der, respectively, and the basement membrane zone is indicated by a red line. In the left panel, the area of the white rectangle is shown enlarged at the lower right. Red asterisk: anchoring fibril; Epi: epidermis; Der: dermis; BMZ: basement membrane zone. Scale bars: 2 μm. **b,** Representative immunofluorescence images of skin specimens from five healthy controls and 11 patients with generalized vitiligo stained with anti-collagen IV (green), anti-TRP1 (red), and DAPI (blue). The areas in the white rectangles are shown in the corresponding right panels. Scale bar: 100 μm. **c,** Representative immunoelectron microscopy images of frozen sections stained with anti-collagen IV. White arrowhead: collagen IV-labeled gold-particle deposits close to the lamina densa; White arrow: collagen IV-labeled gold-particle deposits close to the branched structure of lamina densa; White asterisk: collagen IV-labeled gold-particle deposits close to the layered structure of lamina densa. Scale bars: 1 μm.

Figure 2. Matrix metalloproteinase 2 expression is elevated in the dermis of

430 **vitiliginous skin**

431 **a,** Representative immunofluorescence images of frozen sections of skin from five healthy controls
432 and 11 patients with generalized vitiligo. MMP2 is stained green, and MMP9 is stained red. Vitiligo-
433 L: lesional vitiliginous skin. **b,** Quantitation of MMP2 and MMP9 expression by fluorescence intensity
434 measurement. **c,** Representative immunofluorescence staining of MMP2, HSP47, and CD31 in skin
435 from healthy controls and patients with vitiligo. **d,** Quantitation of fibroblast and endothelial cell
436 numbers in healthy and vitiliginous skin. **e,** Quantitation of $MMP2^+$ fibroblast and $MMP2^+$ endothelial
437 cell numbers. **f,** The ratios of $MMP2^+$ fibroblasts among all fibroblasts and $MMP2^+$ endothelial cells
438 among all endothelial cells. **g,** Representative immunofluorescence staining of $MMP2^+$ fibroblasts
439 distributed around the BM. MMP2 is stained red; the fibroblast marker HSP47 is stained green; and
440 collagen IV, the main component of BM, is stained blue. White arrowhead: $MMP2^+$ fibroblasts close
441 to the BM; White arrow: $MMP2^+$ fibroblasts passed through the BM. **h,** Western blot analyses showing
442 expression of the pro and active forms of MMP2 in skin lysates from healthy skin and lesional
443 vitiliginous skin. **i,** Quantitation of active MMP2 and total MMP2 (the total of active and pro MMP2)
444 expression according to western blot data. Nuclei are counterstained in blue with DAPI in **a** and **c**.
445 Scale bars in **a** and **c**: 50 μm. Scale bars in **g**: 20 μm.

446 **Figure 3. Overexpression of MMP2 in dermal fibroblasts results in melanocyte**
447 **disappearance in three-dimensional human full-thickness skin equivalent and**

448 **human *ex vivo* cultured skin explants.**

449 **a,** Schematic flow diagram depicting the reconstructed three-dimensional human skin full-thickness
450 equivalent model. **b,** Macroscopic images of skin equivalents. **c,** Representative immunofluorescence
451 staining of the melanocyte marker TRP1 and the BM marker laminin 332 in skin equivalents. TRP1
452 is stained red, and laminin 332 is stained green. Nuclei are counterstained in blue with DAPI. **d,**
453 Schematic diagram of the human skin explant culture model. **e,** Representative immunofluorescence
454 staining of collagen IV and melan-A in cultured human skin explants. Collagen IV is stained blue, and
455 melan-A is stained green. Intradermally injected fibroblasts are labeled with PKH fluorescent dye in
456 red. The white rectangle outlines the area of melanocytes and BM, and the detail is shown in the
457 corresponding lower panel. Scale bars in **c** and **e**: 50 μm. Data in **b**, **d**, **e**, **f,** and **i** are shown as mean ±
458 standard deviation.

459 **Figure 4. Melanocyte disappearance results from decreased adhesion to the BM in**
460 **the three-dimensional skin equivalent model.**

461 **a,** Representative immunofluorescence staining of TRP1 and cleaved-caspase 3 in three-dimensional
462 skin equivalents. TRP1 is stained green, and cleaved-caspase 3 is stained red. Mock-Fb indicates skin
463 equivalent embedded with mock-transfected fibroblasts; MMP2-Fb (MZ) indicates the marginal zone
464 of skin equivalent embedded with MMP2-overexpressing fibroblasts. Detached melanocytes are
465 shown by white arrows. **b,** Schematic diagram of the proximity ligation assay and melanocyte antibody

466 cocktail immunofluorescence co-staining. **c,** The interactions between DDR1 and collagen IV and
467 between integrin β1 and laminin in skin equivalents are visualized in red fluorescence by proximity
468 ligation assay. Melanocytes are visualized in green. Nuclei are counterstained in blue with DAPI. The
469 areas in the white rectangles are shown at the lower right. **d,** Quantitation of the fluorescence intensity
470 around melanocytes in proximity ligation assays of five skin equivalents. Scale bars in **a** and **c**: 50 μm.
471 Data in **d** are shown as mean ± standard deviation.

472 **Figure 5. Melanocyte disappearance results from decreased adhesion to the BM in**
473 **vitiliginous skin.**

474 **a,** Representative immunofluorescence staining of TRP1 in healthy skin and perilesional vitiliginous
475 skin. TRP1 is stained red. Nuclei are counterstained in blue with DAPI. Detached melanocytes are
476 shown by white arrows. Vitiligo-PL indicates perilesional vitiliginous skin. **b,** Representative
477 immunofluorescence staining of DDR1, collagen IV, and TRP1 in healthy skin and perilesional
478 vitiliginous skin. DDR1 is stained green, collagen IV is stained blue, and TRP1 is stained red. The
479 area in the white rectangle is shown on the lower right. The red lines circling the areas in the enlarged
480 images indicate melanocytes. **c,** Representative immunofluorescence staining of integrin β1, laminin,
481 and TRP1 in healthy skin and perilesional vitiliginous skin. Integrin β1 is stained green, laminin is
482 stained blue, and TRP1 is stained red. The area in the white rectangle is shown on the lower right. **d,**
483 Schematic diagram of the proximity ligation assay and melanocyte antibody cocktail

484 immunofluorescence co-staining. **e,** The interactions between DDR1 and collagen IV and between
485 integrin β1 and laminin are visualized in red fluorescence by proximity ligation assay. Melanocytes
486 are visualized in green. Nuclei are counterstained in blue with DAPI. The area in the white rectangle
487 is shown on the lower right. **f,** Quantitation of the immunofluorescence signal around melanocytes in
488 **b** and **c**. **g,** Quantitation of the fluorescence intensity around melanocytes in proximity ligation assays
489 in **e**. **h,** Illustration of melanocyte–BM adhesion in healthy skin and vitiliginous skin. Scale bars in **a,**
490 **b, c,** and **e**: 50 μm. Data in **f** and **g** are shown as mean ± standard deviation.

491 **Figure 6. Compensatory enhanced hemidesmosome adhesion in the basal**
492 **keratinocytes of vitiliginous skin.**

493 **a,** Representative immunofluorescence staining of integrin α6, laminin, and TRP1 in healthy skin and
494 lesional vitiliginous skin. Integrin α6 is stained green, laminin is stained blue, and TRP1 is stained red.
495 The area in the white rectangle is shown on the lower right. **b,** Representative immunofluorescence
496 staining of collagen XVII, collagen IV, and TRP1 in healthy skin and lesional vitiliginous skin.
497 Collagen XVII is stained green, collagen IV is stained blue, and TRP1 is stained red. The area in the
498 white rectangle is shown on the lower right. **c,** Quantitation of the immunofluorescence signal around
499 basal keratinocytes in **a** and **b**. **d,** Schematic diagram of the proximity ligation assay. **e,** The interactions
500 between integrin α6 and laminin and between collagen XVII and collagen IV are visualized in red
501 fluorescence by proximity ligation assay. Nuclei are counterstained in blue with DAPI. The area in the

502 white rectangle is shown on the lower right. **f,** Quantitation of the fluorescence intensity around basal
503 keratinocytes in the proximity ligation assays in **e**. **g,** Illustration of basal keratinocyte–BM adhesion
504 in healthy skin and vitiliginous skin. Scale bars in **a, b,** and **e**: 50 μm. Data in **c** and **f** are shown as
505 mean ± standard deviation.

506 **Figure 7. The decreased adhesion of melanocytes to the BM is due to abnormal BM**
507 **architecture.**

508 **a,** Representative ultrastructural images of ultrathin sections of skin from five healthy controls and
509 five patients with generalized vitiligo. An enlarged image of the area indicated by the red arrowhead
510 is shown on the lower right. The red double arrow indicates the lamina lucida. Epi: epidermis; Der:
511 dermis. Scale bars: 1 μm. **b,** Representative immunoelectron microscopy images of ultrathin skin
512 sections stained with anti-laminin antibody. The area of the lamina lucida is outlined in yellow. Scale
513 bars: 1 μm. **c,** Quantitation of the width of the lamina lucida in **a**. Three measurements were performed
514 per section. **d,** Quantitation of the ratio of the number of laminin gold particles located at the lamina
515 lucida to the length of the lamina lucida. **e,** Illustration of melanocyte–BM adhesion in healthy skin
516 and vitiliginous skin. Data in **c** and **d** are shown as mean ± standard deviation.

517 **Figure 8. Subcutaneous inoculation of mice with MMP2-overexpressing fibroblasts**

518 **induced a vitiligo phenotype that could be reversed by inhibition of MMP2**

519 **a,** Schematic diagram of the subcutaneous fibroblast inoculation mouse model. **b,** Macro appearance
520 of the mice at 3 weeks after fibroblast inoculation. The bottom panels show the corresponding
521 threshold binarization images of the back skin of the mice. **c,** Representative immunofluorescence
522 staining of TRP1, HSP47, and collagen IV in mouse skin sections. TRP1 is stained red, HSP47 is
523 stained green, and collagen IV is stained blue. The area in the white rectangle is shown in the
524 corresponding lower panel. Scale bars: 50 μm. **d,** Schematic of the experimental procedure to treat
525 mice with MMP2 inhibitor. **e,** Macroscopic images of the mice at 2 weeks after subcutaneous
526 inoculation. The bottom panels show the corresponding threshold binarization images of the back skin
527 of the mice. **f,** Quantitation of the ratio of depigmentation area on the back skin of the mice. Data in **f**
528 are shown as mean ± standard deviation.

529 **Figure 9. Summary illustration of MMP2-induced melanocyte disappearance in**
530 **vitiligo.**

531 Schematic representation of normal skin and vitiliginous skin. Melanocytes are located at the basal
532 layer of the epidermis interacting with the BM. In normal skin, laminin is normally distributed on
533 collagen IV. Basal melanocytes attach to the BM mainly by integrin β1–laminin binding. In
534 vitiliginous skin, collagen IV is degraded into fragments by the increased $MMP2^{+}$ dermal fibroblasts,
535 the laminin distribution is disrupted, and it is difficult for basal melanocytes to attach to the BM

536 through integrin β1–laminin binding. Melanocytes detach from the BM and disappear from the
537 epidermis. Although integrin β1–laminin binding and integrin α6–laminin binding are diminished in
538 basal keratinocytes of vitiliginous skin, collagen XVII–collagen IV binding is enhanced as a
539 compensatory mechanism.

Materials & Methods

Human skin specimens

Histo-immunofluorescence staining was performed with frozen biopsy samples obtained from lesional and perilesional skin of well-defined patients with non-segmental vitiligo (n = 13, 7 in progressive state and 4 in stable state) (**Table 1**) and from corresponding sites on healthy donors (n = 5; 2 from the abdomen, 2 from an arm, and 1 from the chest). Three-millimeter punch fresh skin biopsy specimens of lesional skin from confirmed patients with vitiligo (n = 3) and samples from corresponding sites on healthy donors (n = 3) were used for protein extraction. One-millimeter punch skin biopsy specimens of lesional skin from confirmed patients with vitiligo (n = 5) and samples from corresponding sites on healthy donors (n = 5) were used for electron microscopy and immuno-electron microscopy analyses. The progressive state of vitiligo was defined by the development of new lesions or the extension of pre-existing lesions in the last 6 months, and the stable state was defined by no increase in the size of existing lesions and an absence of new lesions in the past 1 year. Written informed consent was obtained from all participants prior to study inclusion. The study was approved by the Medical Ethics Committee of Osaka Metropolitan University (No. 4152).

Fluorescent Immunohistochemistry Staining

Human skin tissue and 3D skin samples embedded in OCT compound (Sakura Fineteck, Tokyo, Japan) were cut into 6-μm sections for immunohistochemistry analyses. After fixation with 4%

558 paraformaldehyde (163-20145, Wako, Osaka, Japan) for 10 min and blocking with 5% BSA for 30
559 min at room temperature, these sections were incubated with 1:100 diluted primary antibodies specific
560 for collagen IV (ab6586, Abcam, Cambridge, MA, USA), TRP1 (SIG-38150, Bio Legend, San Diego,
561 CA, USA), MMP2 (ab86607, Abcam), MMP9 (ab119906, Abcam), HSP47 (ADI-SPA-470, Enzo Life
562 Sciences, Farmingdale, NY, USA), CD31 (M0823, Dako, Santa Clara, CA, USA), laminin 332
563 (ab78286, Abcam), melan-A (SIG-38160, Bio Legend), cleaved-caspase 3 (#9664, Cell Signaling
564 Technology, Danvers, MA, USA), DDR1 (PA5-29284, Thermo Fischer Scientific, Waltham, MA,
565 USA), integrin β1 (ab30388, Abcam), Laminin (ab11575, Abcam), integrin α6 (ab20142, Abcam),
566 and collagen XVII (HPA043673, Sigma-Aldrich, Burlington, MA, USA) and then with the appropriate
567 secondary antibody (Alex Fluor 488/555/647 anti-rabbit IgG, anti-mouse IgG1, anti-mouse IgG2a,
568 anti-mouse IgG2b, or anti-goat IgG; 1:1,000, Invitrogen, Grand Island, NY, USA). Nuclei were
569 counterstained with DAPI (#62248, Thermo Fischer Scientific). Murine skin tissues embedded in OCT
570 compound were cut into 6-μm sections for immunohistochemistry analyses. After fixation and
571 blocking, these sections were incubated with 1:100 diluted primary antibodies specific for TRP1 (SIG-
572 38150, Bio Legend), HSP47 (ADI-SPA-470, Enzo Life Sciences), and collagen IV (ab19808, Abcam),
573 and then with the appropriate secondary antibody (Alex Fluor 488 anti-mouse IgG2b, Alex Fluor 555
574 anti-mouse IgG2a, or Alex Fluor 647 anti-rabbit IgG; 1:1,000, Invitrogen). Slides were observed using
575 an LSM 710 Zeiss confocal laser microscope. Images were captured using Zeiss ZEN 2012 software

576 (Carl Zeiss Inc., Jena, Germany). Counting of positively stained cells and measurement of mean
577 fluorescence intensity were carried out using Image J Software (NIH,
578 http://rsb.info.nih.gov/ij/index.html).

579 **Electron Microscopy**

580 Punch biopsy skin samples (1 mm) were fixed with 2.5% glutaraldehyde in 0.1 M phosphate-
581 buffered saline (PBS) at pH 7.4 for 2 h and then washed overnight with PBS. Samples were then post-
582 fixed in 1% O_sO_4 (157-01141, Wako) in PBS for 1h. After washing with DDW, samples were
583 dehydrated with a graded ethanol series and embedded in EPON (TAAB EPON, 342-2, Nisshin EM,
584 Tokyo, Japan). Ultrathin sections (70–80 nm) were cut and transferred to grids, dual-stained with
585 uranyl acetate and lead citrate, and visualized on an FEI Talos F200C G2 Transmission Electron
586 Microscope (Thermo Fisher Scientific). The width of lamina lucida was measured using Image J
587 Software (NIH, http://rsb.info.nih.gov/ij/index.html).

588 **Pre-Embedding Immunoelectron Microscopy**

589 Pre-embedding gold enhancement immunogold labeling was performed as detailed previously[66]
590 with a slight modification. Briefly, skin tissues were fixed in 4% paraformaldehyde (163-20145,
591 Wako) for 30 min at room temperature and embedded in OCT compound. Frozen sections (7 μm) were
592 permeabilized in 0.25% saponin (47036, Sigma-Aldrich) for 30 min and then blocked for 30 min in
593 PBS containing 0.1% saponin, 10% bovine serum albumin (013-25773, Wako), 10% normal goat

594 serum (16210-072, Thermo Fisher Scientific), and 0.1% cold water fish skin gelatin (G7041, Sigma-
595 Aldrich). Samples were incubated with anti-collagen IV (1:100; ab19808, Abcam) or anti-laminin
596 (1:100; ab11575, Abcam) overnight at 4°C in a blocking solution and then with colloidal gold-
597 conjugated anti-rabbit IgG (1.4-nm diameter; 1:200; #2003, Nanoprobes, Yaphank, NY, USA) in a
598 blocking solution for 2 h at room temperature. The signal was intensified with the Gold Enhancement
599 EM Kit (#2113, Nanoprobes) for 4 min at room temperature. The specimens were post-fixed in 1%
600 OsO4, dehydrated in a series of graded ethanol solutions, and embedded in EPON (TAAB EPON,
601 342-2, Nisshin EM). Ultrathin sections (70 nm) were collected and stained with uranyl acetate and
602 lead citrate. Images were taken with an FEI Talos F200C G2 Transmission Electron Microscope
603 (Thermo Fisher Scientific) equipped with an Advanced Microscopy Techniques charge-coupled
604 device-based camera system. The quantitation analyses of positive gold particles were carried out
605 using Image J Software (NIH, http://rsb.info.nih.gov/ij/index.html).

606 **Western Blot Analyses**

607 For the preparation of protein samples, punch fresh skin biopsy specimens were extracted as
608 described previously[67]. Five micrograms of extracted protein was used for western blot analysis with
609 primary antibody against MMP2 (1:200; ab92536, Abcam). The signal intensity of bands was
610 quantified using the Image J densitometry software (NIH).

611 **Cell Culture and Establishment of MMP2-Overexpressing Cells**

612 Normal human dermal fibroblasts (Neonatal, Primary, FC-0001, Lifeline Cell Technology, Carlsbad,
613 CA, USA) were maintained in MEM (M4655, Sigma-Aldrich) with 1% NEAA (139-15651, Wako),
614 5% FBS (10270-106, Gibco, Thermo Fisher Scientific), 1 mM Sodium Pyruvate (11360-070, Gibco,
615 Thermo Fisher Scientific), and 1% penicillin/streptomycin (168-23191, Wako). C57BL/6 mouse
616 dermal fibroblasts (Neonatal, Primary, SCR-M230057, ScienCell Research Laboratories, Carlsbad,
617 CA, USA) were maintained in Fibroblast Medium-2 (2331, ScienCell Research Laboratories). Cells
618 were incubated at 37°C in a humidified incubator supplied with 5% CO_2.

619 Normal human dermal fibroblasts and C57BL/6 mouse dermal fibroblasts (2×10^6 cells/well on 10-
620 cm plates) were transfected with 20 μg human MMP2 expression or murine MMP2 expression
621 episomal vector DNA or empty episomal vector DNA (customized pEBMulti-Puro, Fujifilm Wako
622 Pure Chemical Corporation, Osaka, Japan) mixed with P3000 and Lipofectamine 3000
623 (Lipofectamine™ 3000, Thermo Fisher Scientific). Successfully transfected cells were selected with
624 1 μg/ml puromycin according to the manufacturer's instructions. The expression of the MMP2 proteins
625 in cell lysate and culture medium were confirmed by western blot analyses using antibody against
626 MMP2 (ab92536, Abcam).

627 **Reconstructed Three-Dimensional Human Full-Thickness Skin Equivalents**

628 A reconstructed 3D human full-thickness skin equivalent model was generated as described

629 previously[68] with modification. Collagen gels were prepared from an acid collagen solution (IAC-50,
630 Koken Ltd., Tokyo, Japan) according to the manufacturer's protocol. Then, 2.5×10^5 fibroblasts were
631 cultured on collagen gel in MEM (M4655, Sigma-Aldrich) with 1% NEAA (139-15651, Wako), 5%
632 FBS (10270-106, Gibco, Thermo Fisher Scientific), 1 mM sodium pyruvate (11360-070, Gibco,
633 Thermo Fisher Scientific), and 1% penicillin/streptomycin (168-23191, Wako). This medium was
634 changed every other day after fibroblast mounting. Two days after the dermal component was prepared,
635 a cell suspension of 8.4×10^5 keratinocytes and 1.2×10^5 melanocytes in 60 μl medium composed of
636 a 1:1 mixture of Epilife and Medium 254 was seeded onto the concave surface of the contracted gel.
637 After 30 min, 2 ml culture medium was added to the inside and outside of the transwell, and the
638 submerged culture was maintained for 2 days. The culture medium was composed of DMEM/F-12
639 (3:1 vol/vol; D5921, N4888, Sigma-Aldrich) containing 0.3% FCS, 0.1 mM ethanolamine, 0.1 mM *o*-
640 phosphoethanolamine, 0.4 μg/ml hydrocortisone, 5 μg/ml insulin, 0.09 mM adenine, 5 μg/ml
641 transferrin, 20 pM triiodothyronine, 0.64 mM choline chloride, 0.675 mM serine, 20 μg/ml linoleic
642 acid/BSA, 50 μg/ml ascorbic acid, 7.25 mM glutamine, 10 nM progesterone, 100 I.U./ml penicillin,
643 and 100 μg/ml streptomycin. The thus-formed early skin equivalents were then raised to the air-liquid
644 interface and placed in cornification medium composed of a 1:1 mixture of Ham's F-12 and DMEM
645 supplemented with 0.3% FCS, 0.1 mM ethanolamine, 0.1 mM *o*-phosphoethanolamine, 0.4 μg/ml
646 hydrocortisone, 5 μg/ml insulin, 0.09 mM adenine, 5 μg/ml transferrin, 20 pM triiodothyronine, 0.64

647 mM choline chloride, 0.75 mM serine, 20 μg/ml linoleic acid/BSA, 50 μg/ml ascorbic acid, 7.25 mM
648 glutamine, 0.75 mM calcium chloride, 100 I.U./ml penicillin, and 100 μg/ml streptomycin. The
649 medium was subsequently changed every other day. One week after the air-liquid interface incubation,
650 the skin equivalents were harvested and subjected to macroscopic examination and further histology
651 analyses. All skin equivalent experiments were performed in quintuplicate in five transwells.

652 To prepare the half-half 3D human skin equivalent, MMP2-overexpressing fibroblasts embedded in
653 collagen gel were incubated at 37℃ for 30 min. The early-formed dermal tissue construct was then
654 cut into half size and transferred to one side of a culture transwell insert, and freshly prepared collagen
655 solution containing normal fibroblasts was injected into the other side of the transwell insert. After 2
656 days of culture, keratinocytes and melanocytes were seeded as described above.

657 **Ex Vivo Human Skin Explant Culture**

658 Skin from the lateral abdomen was obtained with the informed consent of patients undergoing
659 abdomen reduction surgery, in accordance with the ethical guidelines of the Research Ethics
660 Committee of Osaka Metropolitan University (No. 4152). The explants were cut (1.0 cm^2) and cultured
661 at an air-liquid interface on culture inserts (filter pore size 8 μm; #141082, Thermo Fisher Scientific)
662 with a 1:1 mixture of Ham's F-12 and DMEM supplemented with 0.3% FCS, 0.1 mM ethanolamine,
663 0.1 mM *o*-phosphoethanolamine, 0.4 μg/ml hydrocortisone, 5 μg/ml insulin, 0.09 mM adenine, 5
664 μg/ml transferrin, 20 pM triiodothyronine, 0.64 mM choline chloride, 0.75 mM serine, 20 μg/ml

665 linoleic acid/BSA, 50 μg/ml ascorbic acid, 7.25 mM glutamine, 0.75 mM calcium chloride, 100
666 I.U./ml penicillin, and 100 μg/ml streptomycin. The insert was set on a 12-well plate (3401, Corning
667 Inc., Corning, NY, USA) and cultured at 37℃ in a humidified incubator with 5% CO_2 for 7 days.

668 For fibroblast inoculation, normal fibroblasts and MMP2-overexpressing fibroblasts were labeled
669 with the red fluorescent dye PKH26 (MINI26-1KT, Sigma-Aldrich) according to the manufacturer's
670 instructions and then subcutaneously injected into cultured human skin explants at a density of 5×10^6
671 cells/ml in 100 μl using disposable 35G needles (ReactSystem, Osaka, Japan).

672 ***In Situ* Proximity Ligation Assay**

673 Multicolor *in situ* PLA was performed using the Duolink PLA Multicolor detection kit (Duolink®
674 PLA® Multicolor Reagent Pack, DUO96000, Sigma-Aldrich) as described previously[69] with slight
675 modification. Briefly, frozen skin sections were blocked with blocking solution (DUO82007, Duolink,
676 Sigma-Aldrich) for 30 min at 37 °C and then incubated overnight at 4°C with primary antibodies pre-
677 conjugated with Red Oligo A (DUO86010A, Sigma-Aldrich) or Red Oligo B (DUO86010B, Sigma-
678 Aldrich). After washing with Duolink *In Situ* Wash Buffer A (DUO82046, Sigma-Aldrich), ligation
679 and amplification reactions were performed using a Duolink PLA Multicolor detection kit (DUO96000,
680 Sigma-Aldrich).

681 For co-staining with melanocyte marker after amplification and washing, sections were incubated
682 with the Alexa Fluor 488-conjugated antibody cocktail (MART1 + Tyrosinase + gp100) [Alexa Fluor®

683 488] (1:100 dilution; NBP2-34681AF488, Novus Biologics, San Jose, CA, USA) for 2 h. After 30 min
684 of washing with Duolink *In Situ* Wash Buffer B (DUO82048, Sigma-Aldrich), sections were mounted
685 using Duolink *In Situ* Mounting Medium with DAPI (DUO82040, Sigma-Aldrich). Then, slides were
686 observed using an LSM 710 Zeiss confocal laser microscope. Images were captured using Zeiss ZEN
687 2012 software (Carl Zeiss Inc., Jena, Germany). Mean fluorescence intensity measurements were
688 carried out using Image J Software (NIH, http://rsb.info.nih.gov/ij/index.html).

689 **Animals and *In Vivo* Experimental Procedures**

690 Krt14-Kitl mice, a C57BL/6-background congenic strain that expresses membrane-bound stem
691 cell factor under the keratin14 promoter to retain epidermal melanocytes and thus have pigmented
692 skin, were purchased from the RIKEN BioResource Research Center (No. RBRC00694, RIKEN BRC,
693 Tsukuba, Ibaraki, Japan). PBS, Mock-Fbs, or MMP2-Fbs (5×10^6 cells/ml in 100 μl PBS) was
694 subcutaneously injected into the back skin of male 7-week-old Krt14-Kitl mice.

695 For treatment, 5 μM SB-3CT dissolved in DMSO (HY-12354, MedChemExpress, Monmouth
696 junction, NJ, USA) or 5 μM Tanomastat dissolved in DMSO (T006900, Toronto Research Chemicals,
697 Toronto, Canada) was subcutaneously co-injected with Mock-Fbs or MMP2-Fbs (5×10^6/ml in 100
698 μl PBS) into the back skin of Krt14-Kitl mice. Two weeks after these treatments, the back skin of the
699 mice was depilated and photographed, and the depigmentation area (n = 5 mice per group) was
700 measured using binarization and different global thresholding values (Image J Software, NIH,

701 http://rsb.info.nih.gov/ij/index.html). Experiments were conducted in accordance with the Guiding
702 Principles for the Care and Use of Laboratory Animals, and the experimental protocol used in this
703 study was approved by the Committee for Animal Experiments at Osaka Metropolitan University
704 (Permit No. 18042, Osaka, Japan).

705 **Statistical Analysis**

706 Experiments were repeated at least three times. Data are presented as the mean ± standard
707 deviation. One-way analysis of variance with Dunnet's test or unpaired Student's t-test (two-tailed)
708 was used for statistical analyses. A value of $p < 0.05$ indicated statistical significance. All statistical
709 analyses for this study were performed using GraphPad Prism version 8.0.0 for Windows (GraphPad
710 Software Inc., San Diego, CA, USA).
711

Table 1. Clinical characteristics of the patients.

Patient No.	Sex	Age (years)	Type	Biopsy site	Activity
1[§]	M	72	Non-segmental vitiligo	Back	Progressive
2[§]	F	49	Non-segmental vitiligo	Lumbar	Stable
3[*]	M	44	Non-segmental vitiligo	Back	Progressive
4[*]	F	33	Non-segmental vitiligo	Axilla	Progressive
5[*]	F	71	Non-segmental vitiligo	Elbow	Stable
6[§]	F	23	Non-segmental vitiligo	Abdomen	Stable
7[§]	M	30	Non-segmental vitiligo	Lateral abdomen	Progressive
8[§]	F	20	Non-segmental vitiligo	Abdomen	Progressive
9	M	68	Non-segmental vitiligo	Back	Progressive
10	F	49	Non-segmental vitiligo	Abdomen	Progressive
11	F	62	Non-segmental vitiligo	Neck	Stable

*Samples for full skin protein extract were obtained from these three patients.

[§]Samples for electron microscopy were from these five patients.

References

1. Le Poole IC, van den Wijngaard RM, Westerhof W, Dutrieux RP, Das PK. Presence or absence of melanocytes in vitiligo lesions: an immunohistochemical investigation. *J Invest Dermatol* **100**, 816-822 (1993).

2. Picardo M*, et al.* Vitiligo. *Nat Rev Dis Primers* **1**, 15011 (2015).

3. Alikhan A, Felsten LM, Daly M, Petronic-Rosic V. Vitiligo: a comprehensive overview Part I. Introduction, epidemiology, quality of life, diagnosis, differential diagnosis, associations, histopathology, etiology, and work-up. *J Am Acad Dermatol* **65**, 473-491 (2011).

4. Katz EL, Harris JE. Translational Research in Vitiligo. *Front Immunol* **12**, 624517 (2021).

5. Lerner AB. Vitiligo. *J Invest Dermatol* **32**, 285-310 (1959).

6. Bergqvist C, Ezzedine K. Vitiligo: A Review. *Dermatology* **236**, 571-592 (2020).

7. Cichorek M, Wachulska M, Stasiewicz A, Tyminska A. Skin melanocytes: biology and development. *Postepy Dermatol Alergol* **30**, 30-41 (2013).

8. Haass NK, Herlyn M. Normal human melanocyte homeostasis as a paradigm for understanding melanoma. *J Investig Dermatol Symp Proc* **10**, 153-163 (2005).

9. Santiago-Walker A, Li L, Haass NK, Herlyn M. Melanocytes: from morphology to application. *Skin Pharmacol Physiol* **22**, 114-121 (2009).

10. Le Poole IC, van den Wijngaard RM, Westerhof W, Das PK. Tenascin is overexpressed in vitiligo lesional skin and inhibits melanocyte adhesion. *Br J Dermatol* **137**, 171-178 (1997).

11. Costell M*, et al.* Perlecan maintains the integrity of cartilage and some basement membranes. *J Cell Biol* **147**, 1109-1122 (1999).

12. Erickson AC, Couchman JR. Still more complexity in mammalian basement membranes. *J Histochem Cytochem* **48**, 1291-1306 (2000).

750
751 13. Lin CQ, Bissell MJ. Multi-faceted regulation of cell differentiation by extracellular matrix.
752 *FASEB J* **7**, 737-743 (1993).
753
754 14. Walakovits LA, Moore VL, Bhardwaj N, Gallick GS, Lark MW. Detection of stromelysin
755 and collagenase in synovial fluid from patients with rheumatoid arthritis and
756 posttraumatic knee injury. *Arthritis Rheum* **35**, 35-42 (1992).
757
758 15. Checchi V*, et al.* The Role of Matrix Metalloproteinases in Periodontal Disease. *Int J*
759 *Environ Res Public Health* **17**, (2020).
760
761 16. Saarialho-Kere UK, Kovacs SO, Pentland AP, Olerud JE, Welgus HG, Parks WC. Cell-
762 matrix interactions modulate interstitial collagenase expression by human keratinocytes
763 actively involved in wound healing. *J Clin Invest* **92**, 2858-2866 (1993).
764
765 17. Fawzy MM, El Maadawi ZM, Hegazy RA, El Fatah NS. Vitiligo - The story from within:
766 A transmission electron microscopic study before and after narrow-band ultraviolet B.
767 *Ultrastruct Pathol* **40**, 265-275 (2016).
768
769 18. Montes LF, Abulafia J, Wilborn WH, Hyde BM, Montes CM. Value of histopathology in
770 vitiligo. *Int J Dermatol* **42**, 57-61 (2003).
771
772 19. Panuncio AL, Vignale R. Ultrastructural studies in stable vitiligo. *Am J Dermatopathol* **25**,
773 16-20 (2003).
774
775 20. Breathnach AS, Bor S, Wyllie LM. Electron microscopy of peripheral nerve terminals and
776 marginal melanocytes in vitiligo. *J Invest Dermatol* **47**, 125-140 (1966).
777
778 21. Has C, Nystrom A. Epidermal Basement Membrane in Health and Disease. *Curr Top*
779 *Membr* **76**, 117-170 (2015).
780
781 22. Nagase H, Woessner JF, Jr. Matrix metalloproteinases. *J Biol Chem* **274**, 21491-21494
782 (1999).
783
784 23. Yong VW, Krekoski CA, Forsyth PA, Bell R, Edwards DR. Matrix metalloproteinases and
785 diseases of the CNS. *Trends Neurosci* **21**, 75-80 (1998).

24. Ram M, Sherer Y, Shoenfeld Y. Matrix metalloproteinase-9 and autoimmune diseases. *J Clin Immunol* **26**, 299-307 (2006).

25. Song J, *et al.* Focal MMP-2 and MMP-9 activity at the blood-brain barrier promotes chemokine-induced leukocyte migration. *Cell Rep* **10**, 1040-1054 (2015).

26. Agrawal S, *et al.* Dystroglycan is selectively cleaved at the parenchymal basement membrane at sites of leukocyte extravasation in experimental autoimmune encephalomyelitis. *J Exp Med* **203**, 1007-1019 (2006).

27. Leppert D, *et al.* Matrix metalloproteinase-9 (gelatinase B) is selectively elevated in CSF during relapses and stable phases of multiple sclerosis. *Brain* **121 (Pt 12)**, 2327-2334 (1998).

28. Tchetverikov I, *et al.* Matrix metalloproteinases-3, -8, -9 as markers of disease activity and joint damage progression in early rheumatoid arthritis. *Ann Rheum Dis* **62**, 1094-1099 (2003).

29. Konttinen YT, *et al.* Matrix metalloproteinase (MMP)-9 type IV collagenase/gelatinase implicated in the pathogenesis of Sjogren's syndrome. *Matrix Biol* **17**, 335-347 (1998).

30. Liotta LA, Abe S, Robey PG, Martin GR. Preferential digestion of basement membrane collagen by an enzyme derived from a metastatic murine tumor. *Proc Natl Acad Sci U S A* **76**, 2268-2272 (1979).

31. Collier IE, *et al.* H-ras oncogene-transformed human bronchial epithelial cells (TBE-1) secrete a single metalloprotease capable of degrading basement membrane collagen. *J Biol Chem* **263**, 6579-6587 (1988).

32. Kobayashi T, Hattori S, Shinkai H. Matrix metalloproteinases-2 and -9 are secreted from human fibroblasts. *Acta Derm Venereol* **83**, 105-107 (2003).

33. Wang L, *et al.* Matrix metalloproteinase 2 (MMP2) and MMP9 secreted by erythropoietin-activated endothelial cells promote neural progenitor cell migration. *J Neurosci* **26**, 5996-6003 (2006).

822
823 34. Zambruno G, Marchisio PC, Melchiori A, Bondanza S, Cancedda R, De Luca M.
824 Expression of integrin receptors and their role in adhesion, spreading and migration of
825 normal human melanocytes. *J Cell Sci* **105 (Pt 1)**, 179-190 (1993).
826
827 35. Fukunaga-Kalabis M*, et al.* CCN3 controls 3D spatial localization of melanocytes in the
828 human skin through DDR1. *J Cell Biol* **175**, 563-569 (2006).
829
830 36. Ricard AS*, et al.* Study of CCN3 (NOV) and DDR1 in normal melanocytes and vitiligo
831 skin. *Exp Dermatol* **21**, 411-416 (2012).
832
833 37. Reichert-Faria A, Jung JE, Moreschi Neto V, de Castro CC, Mira MT, Noronha L.
834 Reduced immunohistochemical expression of Discoidin Domain Receptor 1 (DDR1) in
835 vitiligo skin. *J Eur Acad Dermatol Venereol* **27**, 1057-1059 (2013).
836
837 38. Gauthier Y, Cario-Andre M, Lepreux S, Pain C, Taieb A. Melanocyte detachment after
838 skin friction in non lesional skin of patients with generalized vitiligo. *British Journal of*
839 *Dermatology* **148**, 95-101 (2003).
840
841 39. Wagner RY*, et al.* Altered E-Cadherin Levels and Distribution in Melanocytes Precede
842 Clinical Manifestations of Vitiligo. *J Invest Dermatol* **135**, 1810-1819 (2015).
843
844 40. Verrando P, Hsi BL, Yeh CJ, Pisani A, Serieys N, Ortonne JP. Monoclonal antibody GB3,
845 a new probe for the study of human basement membranes and hemidesmosomes. *Exp Cell*
846 *Res* **170**, 116-128 (1987).
847
848 41. Kahari VM, Saarialho-Kere U. Matrix metalloproteinases and their inhibitors in tumour
849 growth and invasion. *Ann Med* **31**, 34-45 (1999).
850
851 42. Boukhedouni N*, et al.* Type-1 cytokines regulate MMP-9 production and E-cadherin
852 disruption to promote melanocyte loss in vitiligo. *JCI Insight* **5**, (2020).
853
854 43. Kumar R, Parsad D, Kanwar AJ, Kaul D. Altered levels of Ets-1 transcription factor and
855 matrix metalloproteinases in melanocytes from patients with vitiligo. *Br J Dermatol* **165**,
856 285-291 (2011).
857

858 44. Lei TC, Vieira WD, Hearing VJ. In vitro migration of melanoblasts requires matrix
859 metalloproteinase-2: implications to vitiligo therapy by photochemotherapy. *Pigment Cell*
860 *Res* **15**, 426-432 (2002).
861
862 45. Xu Z*, et al.* Anatomically distinct fibroblast subsets determine skin autoimmune patterns.
863 *Nature* **601**, 118-124 (2022).
864
865 46. Delmas V, Larue L. Molecular and cellular basis of depigmentation in vitiligo patients.
866 *Exp Dermatol* **28**, 662-666 (2019).
867
868 47. Kovacs D*, et al.* Vitiligo Skin: Exploring the Dermal Compartment. *J Invest Dermatol* **138**,
869 394-404 (2018).
870
871 48. Kusano K*, et al.* Regulation of matrix metalloproteinases (MMP-2, -3, -9, and -13) by
872 interleukin-1 and interleukin-6 in mouse calvaria: association of MMP induction with
873 bone resorption. *Endocrinology* **139**, 1338-1345 (1998).
874
875 49. Siwik DA, Chang DL, Colucci WS. Interleukin-1beta and tumor necrosis factor-alpha
876 decrease collagen synthesis and increase matrix metalloproteinase activity in cardiac
877 fibroblasts in vitro. *Circ Res* **86**, 1259-1265 (2000).
878
879 50. Choi JY, Piao MS, Lee JB, Oh JS, Kim IG, Lee SC. Propionibacterium acnes stimulates
880 pro-matrix metalloproteinase-2 expression through tumor necrosis factor-alpha in human
881 dermal fibroblasts. *J Invest Dermatol* **128**, 846-854 (2008).
882
883 51. Overall CM, Wrana JL, Sodek J. Transcriptional and post-transcriptional regulation of 72-
884 kDa gelatinase/type IV collagenase by transforming growth factor-beta 1 in human
885 fibroblasts. Comparisons with collagenase and tissue inhibitor of matrix metalloproteinase
886 gene expression. *J Biol Chem* **266**, 14064-14071 (1991).
887
888 52. Philips N, Keller T, Gonzalez S. TGF beta-like regulation of matrix metalloproteinases by
889 anti-transforming growth factor-beta, and anti-transforming growth factor-beta 1
890 antibodies in dermal fibroblasts: Implications for wound healing. *Wound Repair Regen* **12**,
891 53-59 (2004).
892
893 53. Galis ZS*, et al.* Cytokine-stimulated human vascular smooth muscle cells synthesize a

complement of enzymes required for extracellular matrix digestion. *Circ Res* **75**, 181-189 (1994).

54. Yazlovitskaya EM, *et al.* The laminin-binding integrins regulate nuclear factor kappaB-dependent epithelial cell polarity and inflammation. *J Cell Sci* **134**, (2021).

55. Breitkreutz D, Koxholt I, Thiemann K, Nischt R. Skin basement membrane: the foundation of epidermal integrity--BM functions and diverse roles of bridging molecules nidogen and perlecan. *Biomed Res Int* **2013**, 179784 (2013).

56. Kovacs D, *et al.* Altered epidermal proliferation, differentiation, and lipid composition: Novel key elements in the vitiligo puzzle. *Sci Adv* **8**, eabn9299 (2022).

57. Shiu J, *et al.* Multimodal analyses of vitiligo skin identify tissue characteristics of stable disease. *JCI Insight* **7**, (2022).

58. Moretti S, *et al.* Keratinocyte dysfunction in vitiligo epidermis: cytokine microenvironment and correlation to keratinocyte apoptosis. *Histol Histopathol* **24**, 849-857 (2009).

59. Jung SE, Kang HY, Lee ES, Kim YC. Changes of epidermal thickness in vitiligo. *Am J Dermatopathol* **37**, 289-292 (2015).

60. Ryan MC, *et al.* The functions of laminins: lessons from in vivo studies. *Matrix Biol* **15**, 369-381 (1996).

61. Elshafy Khashaba SA, Elkot RA, Ibrahim AM. Efficacy of NB-UVB, microneedling with triamcinolone acetonide, and a combination of both modalities in the treatment of vitiligo: A comparative study. *J Am Acad Dermatol* **79**, 365-367 (2018).

62. Bayoumi W, *et al.* Effect of a preceding laser dermabrasion on the outcome of combined therapy with narrowband ultraviolet B and potent topical steroids for treating nonsegmental vitiligo in resistant localizations. *Br J Dermatol* **166**, 208-211 (2012).

63. Ezzedine K, Eleftheriadou V, Whitton M, van Geel N. Vitiligo. *Lancet* **386**, 74-84 (2015).

930 64. Marie J, *et al.* Inflammasome activation and vitiligo/nonsegmental vitiligo progression. *Br*
931 *J Dermatol* **170**, 816-823 (2014).
932
933 65. Moretti S, *et al.* New insights into the pathogenesis of vitiligo: imbalance of epidermal
934 cytokines at sites of lesions. *Pigment Cell Res* **15**, 87-92 (2002).
935
936 66. Hayashi-Nishino M, Fujita N, Noda T, Yamaguchi A, Yoshimori T, Yamamoto A. A
937 subdomain of the endoplasmic reticulum forms a cradle for autophagosome formation.
938 *Nat Cell Biol* **11**, 1433-1437 (2009).
939
940 67. Yang F, Yang L, Wataya-Kaneda M, Yoshimura T, Tanemura A, Katayama I. Uncoupling
941 of ER/Mitochondrial Oxidative Stress in mTORC1 Hyperactivation-Associated Skin
942 Hypopigmentation. *J Invest Dermatol* **138**, 669-678 (2018).
943
944 68. Yang L, *et al.* Microbubble-enhanced ultrasound for gene transfer into living skin
945 equivalents. *J Dermatol Sci* **40**, 105-114 (2005).
946
947 69. Phoomak C, *et al.* The translocon-associated protein (TRAP) complex regulates quality
948 control of N-linked glycosylation during ER stress. *Sci Adv* **7**, (2021).
949
950

Figure 1

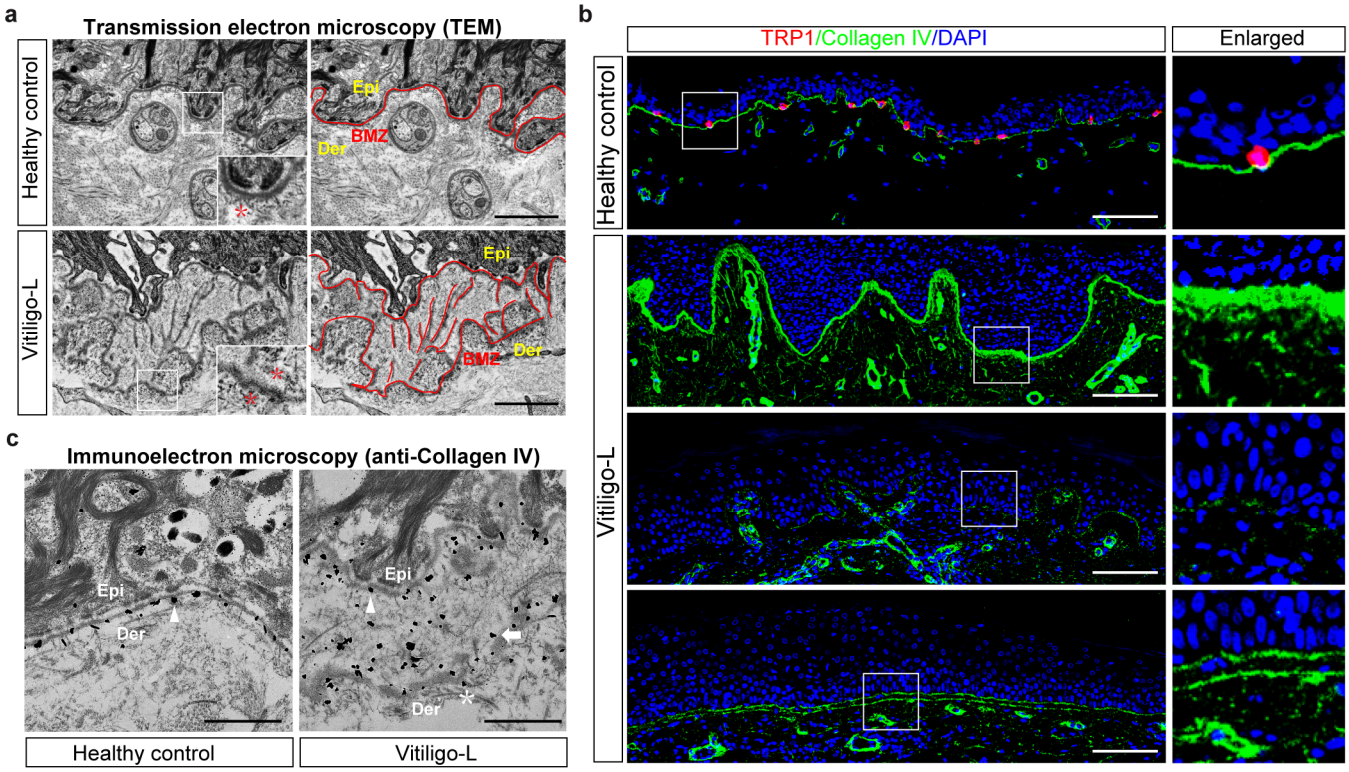

Figure 2

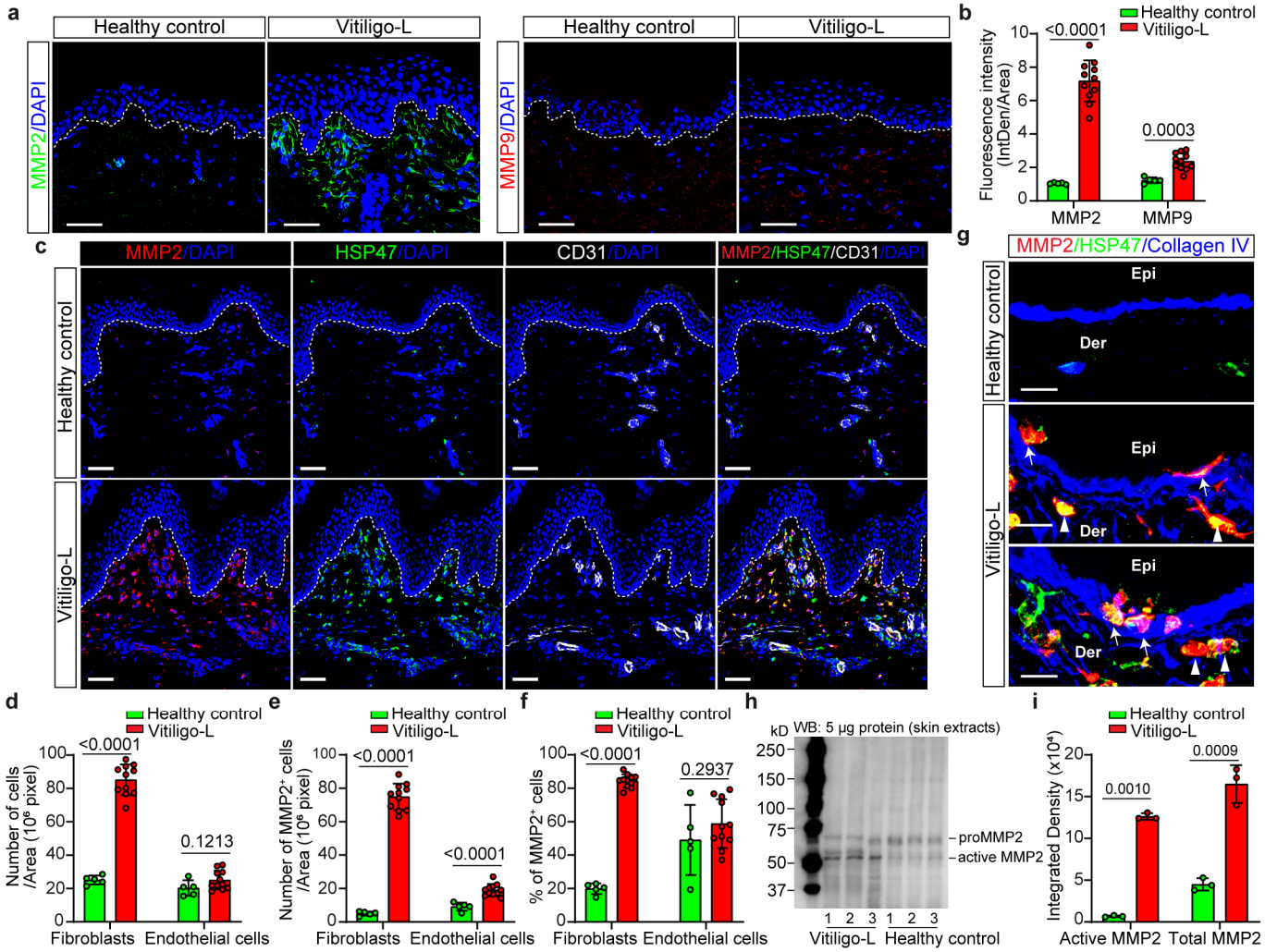

Figure 3

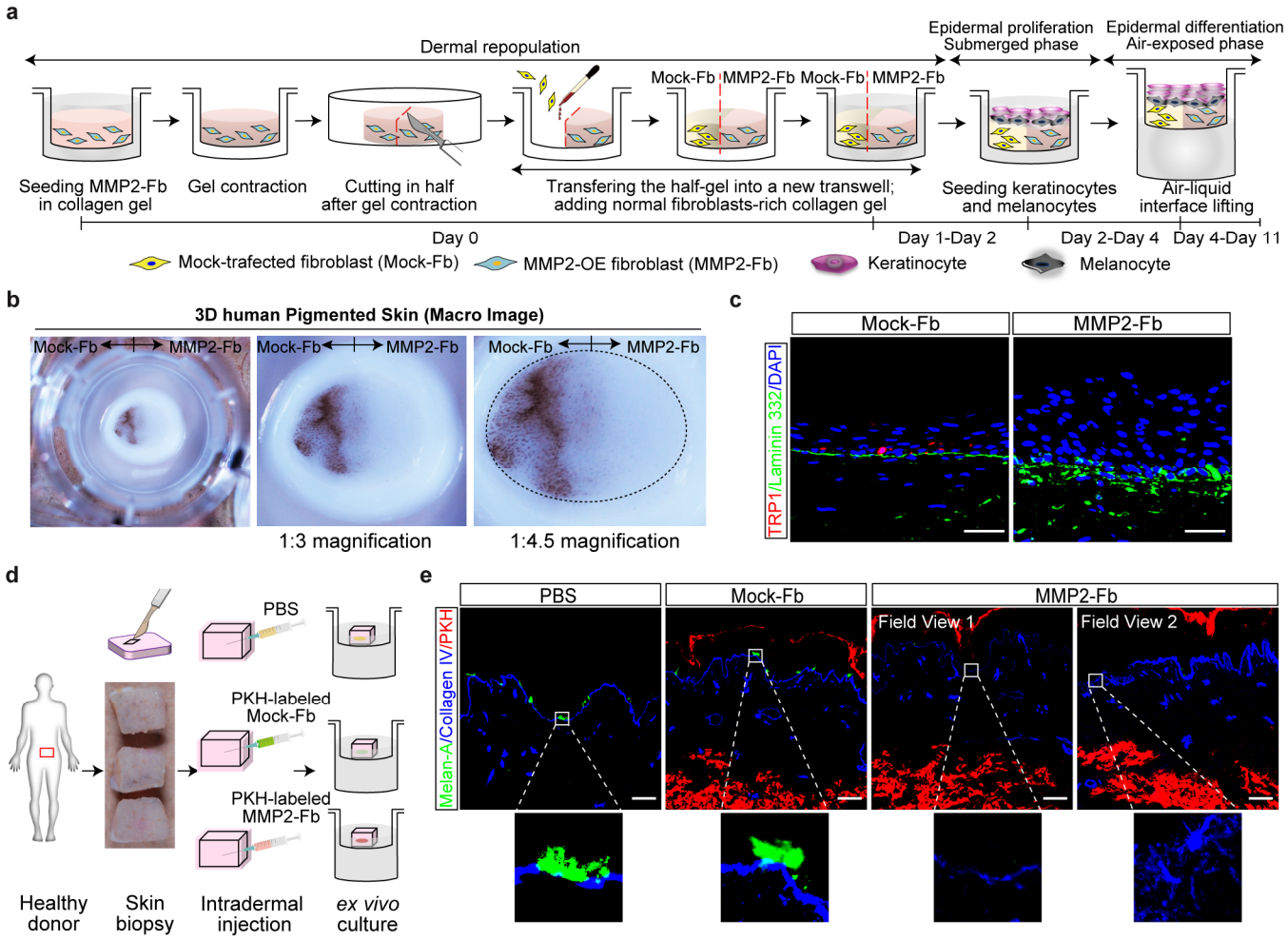

Figure 4

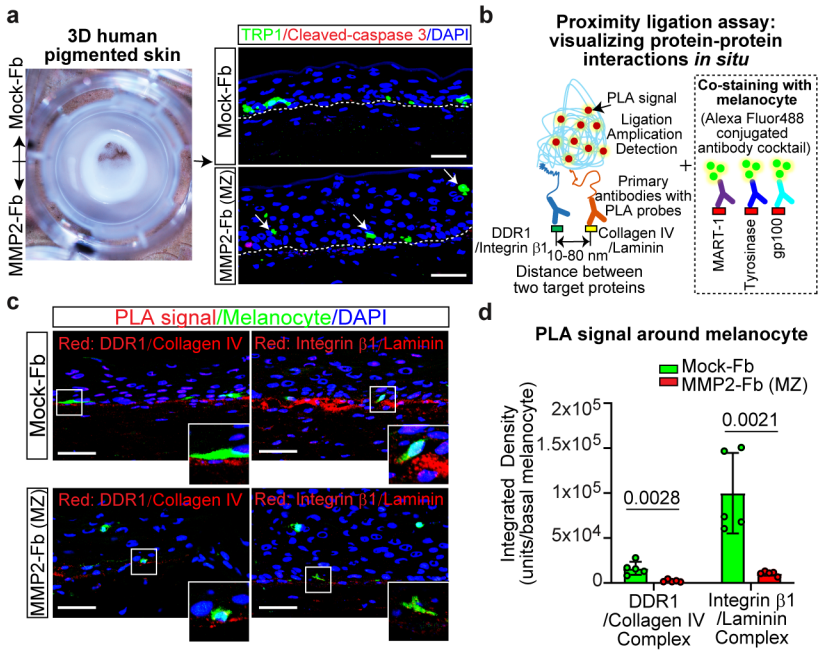

Figure 5

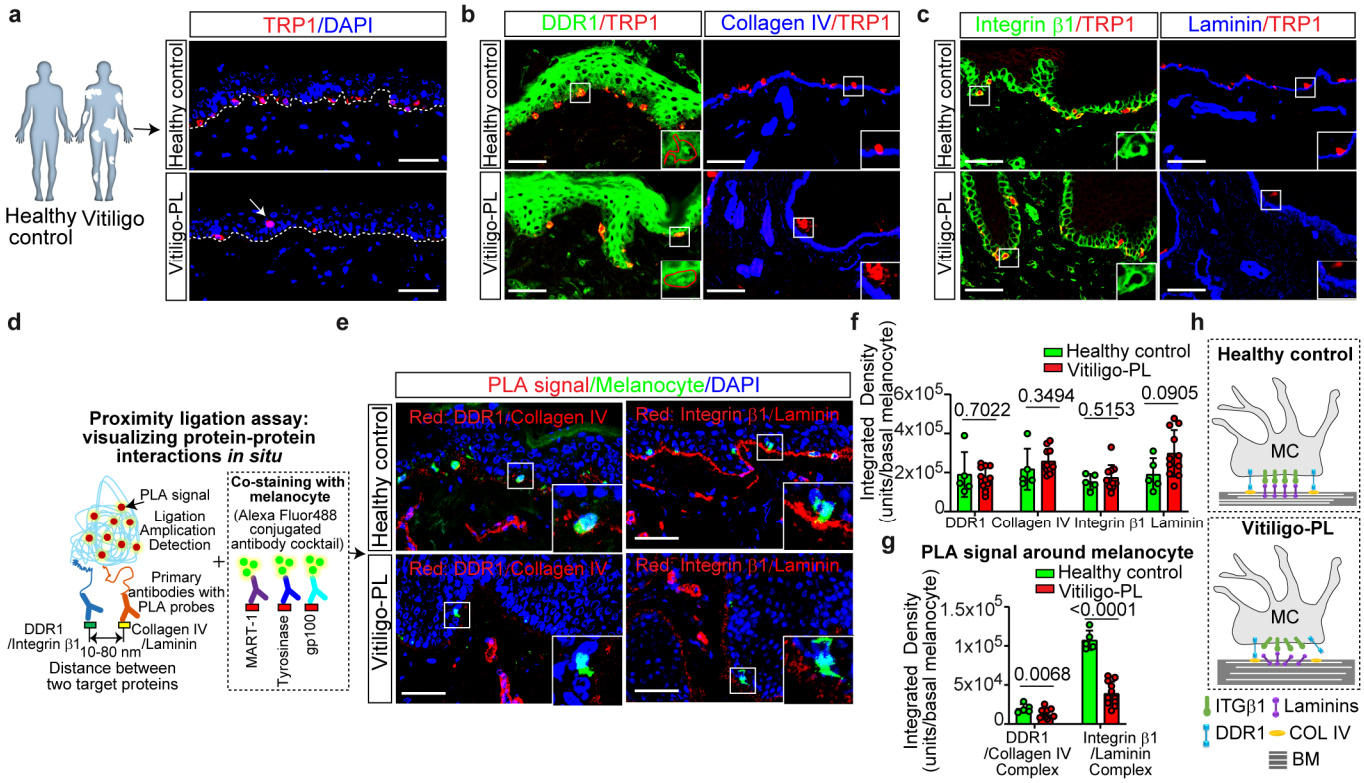

Figure 6

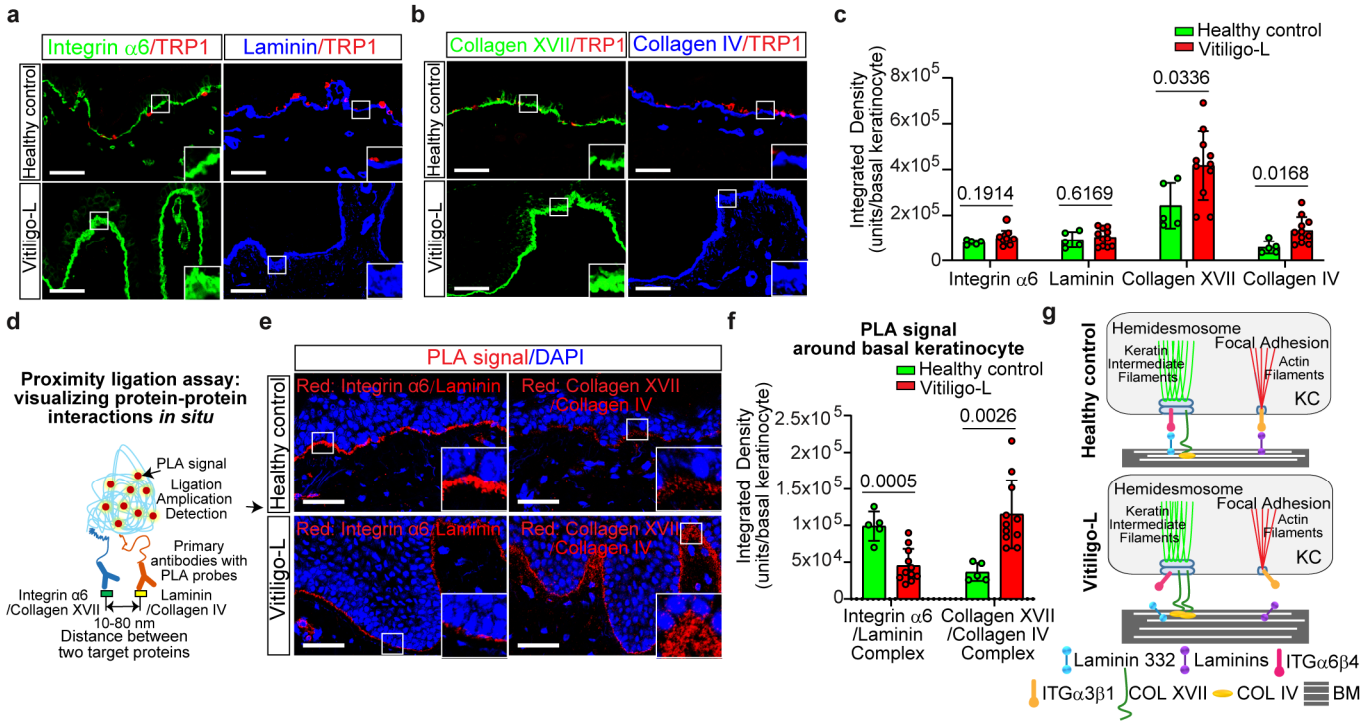

Figure 7

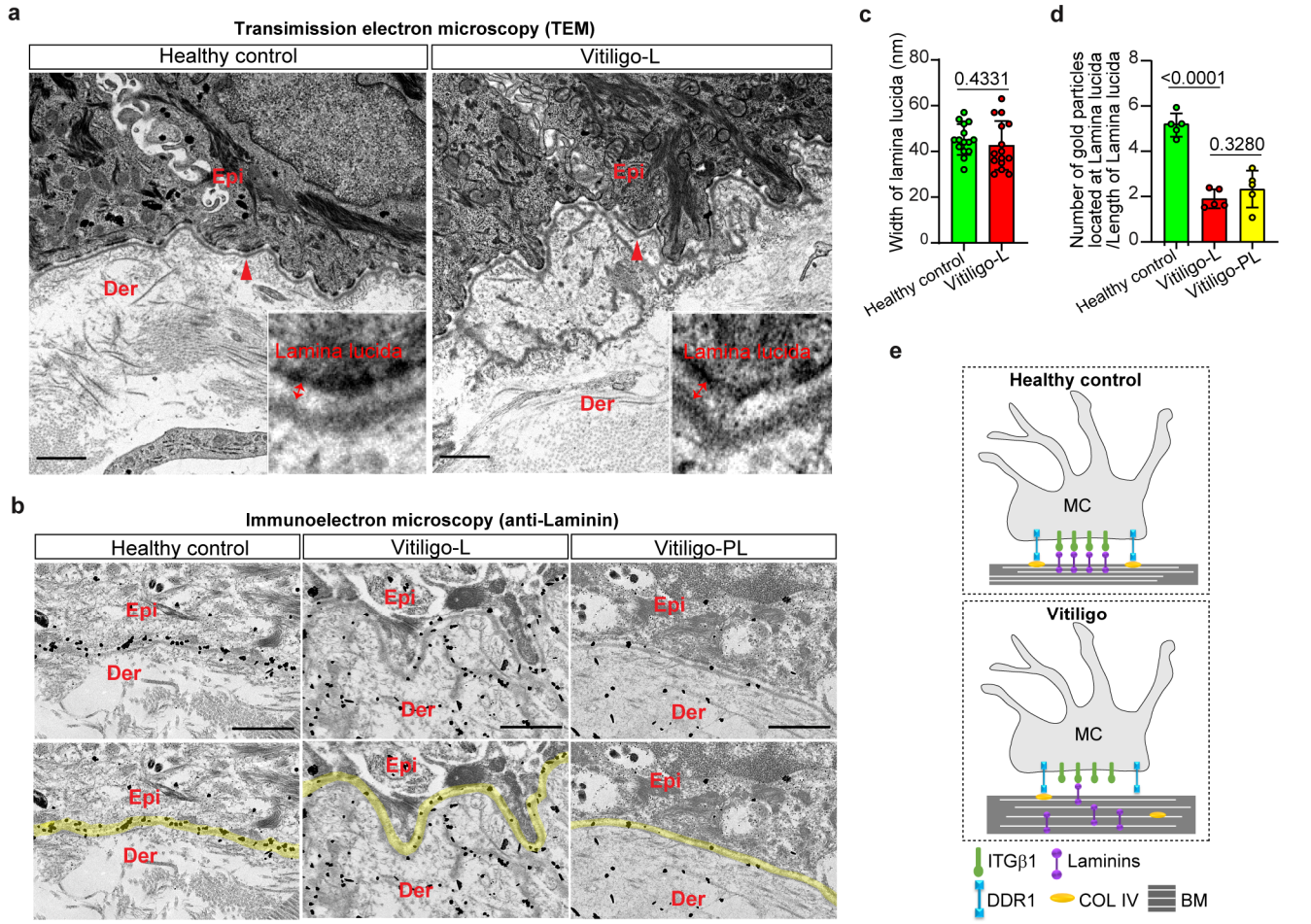

Figure 8

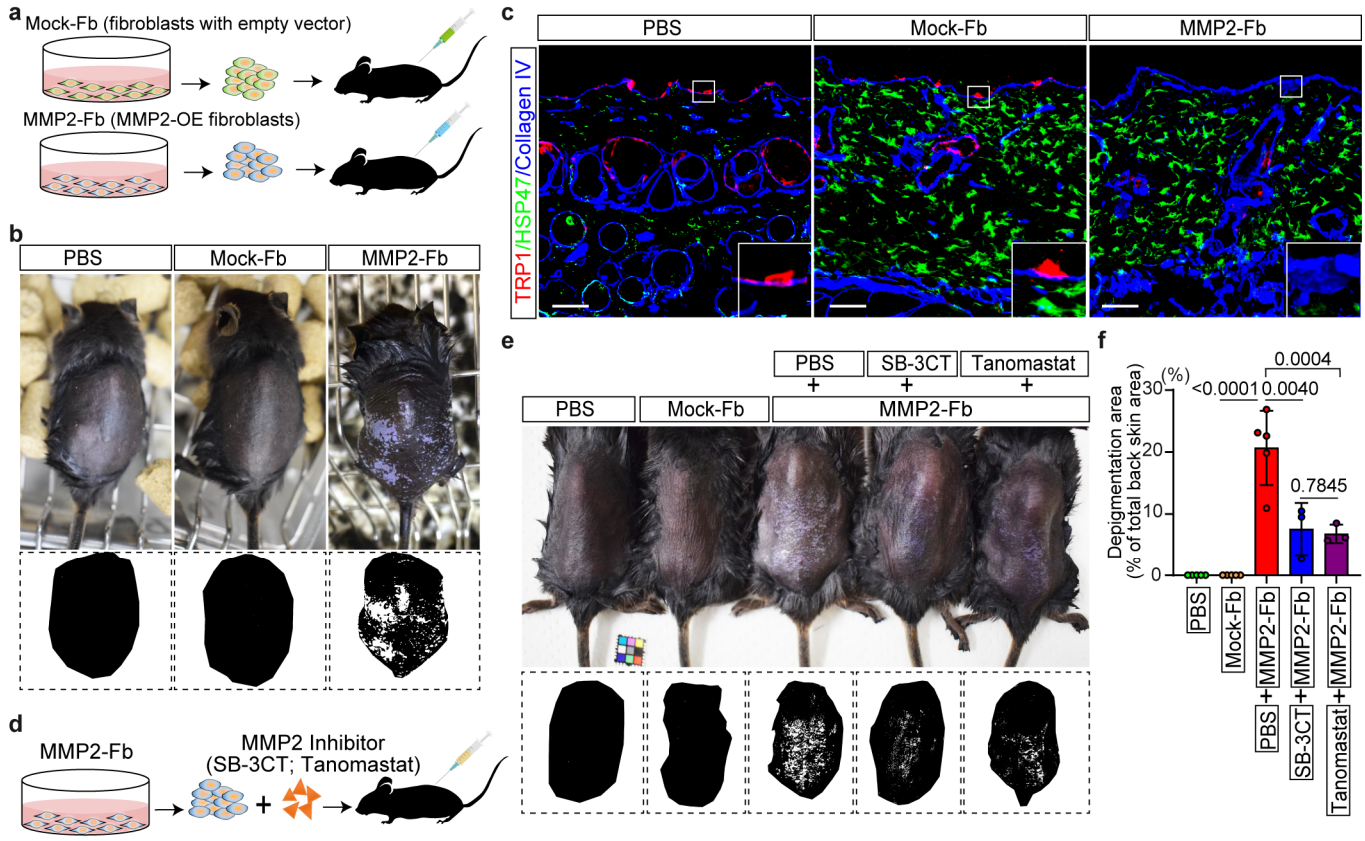

Figure 9

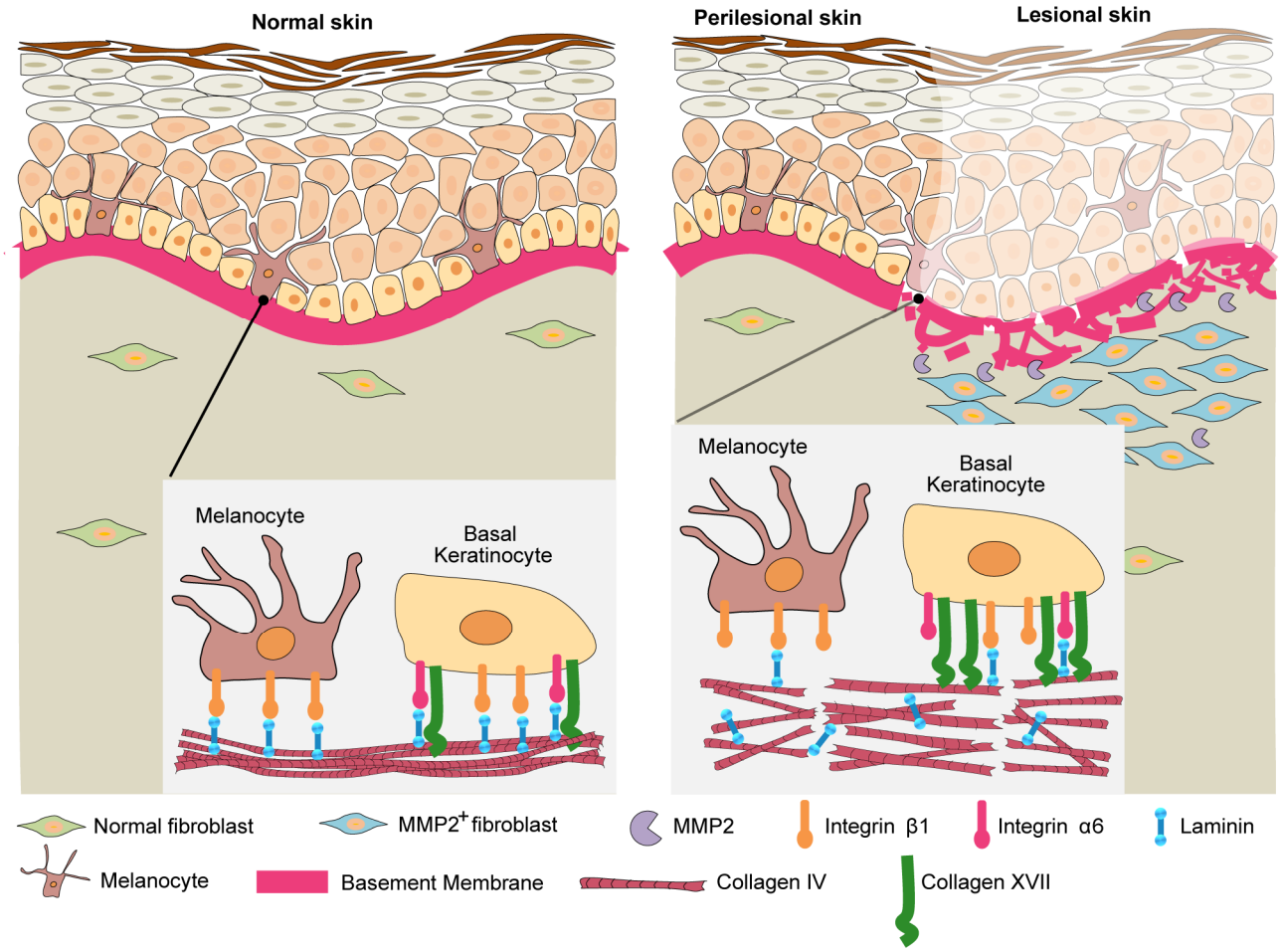
Normal skin
Perilesional skin
Lesional skin
Melanocyte
Basal Keratinocyte
Melanocyte
Basal Keratinocyte
Normal fibroblast
MMP2+ fibroblast
MMP2
Integrin β1
Integrin α6
Laminin
Melanocyte
Basement Membrane
Collagen IV
Collagen XVII

Supplementary Information

Materials & Methods

Fluorescent Immunohistochemistry Staining

Human skin tissue embedded in OCT compound (Sakura Fineteck, Tokyo, Japan) was cut into 6-μm sections for immunohistochemistry analyses. After fixation with 4% paraformaldehyde (163-20145, Wako, Osaka, Japan) for 10 min and blocking with 5% BSA for 30 min at room temperature, these sections were incubated with 1:100 diluted primary antibodies specific for TGF-β1 (ARG66427, Arigobio, Hsinchu, Taiwan), TNF-α (60291-1-Ig, Proteintech, Rosemont, USA), IL-1β (16806-1-AP, Proteintech), and IL-6 (21865-1-AP, Proteintech) and then incubated with the appropriate secondary antibody (Alex Fluor 488/555 anti-rabbit IgG, anti-mouse IgG1, anti-mouse IgG2a; 1:1,000, Invitrogen, Grand Island, NY, USA). Nuclei were counterstained with DAPI (#62248, Thermo Fischer Scientific). Slides were observed using an LSM 710 Zeiss confocal laser microscope. Images were captured using Zeiss ZEN 2012 software (Carl Zeiss Inc., Jena, Germany). Counting of positively stained cells and measurement of mean fluorescence intensity were carried out using Image J Software (NIH, http://rsb.info.nih.gov/ij/index.html).

Figure Legends

Extended Data Fig. 1. Increased cytokine expression in the epidermis of vitiliginous skin

Representative immunofluorescence staining of TGF-β1 (**a**), TNF-α (**b**), IL-1β (**c**), and IL-6 (**d**) in skin sections from healthy controls and lesional skin sections from patients with vitiligo. Nuclei were counterstained in blue with DAPI. The area in the white rectangle is shown on the lower right. Scale bars in **a, b, c**, and **d**: 50 μm.
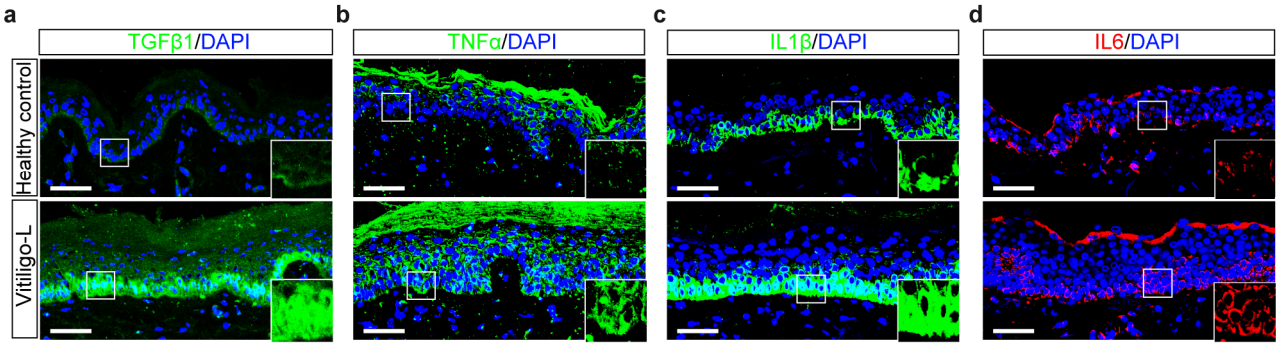
Extended Data Fig. 1